

# Sedimentation processes in silt-rich sediment systems

Steven te Slaa · Qing He · Dirk Sebastiaan van Maren ·  
Johan Christian Winterwerp

Received: 16 June 2012 / Accepted: 30 January 2013 / Published online: 14 March 2013  
© Springer-Verlag Berlin Heidelberg 2013

**Abstract** Sediment found in China's Yangtze and Yellow River systems is characterized by large silt fractions. In contrast to sand and clay, sedimentation and erosion behaviour of silt and silt–clay–sand mixtures is relatively unknown. Therefore, settling and consolidation behaviour of silt-rich sediment from these river systems is analysed under laboratory conditions in specially designed settling columns. Results show that a transition in consolidation behaviour occurs around clay contents of about 10 %, which is in analogy with the transition from non-cohesive to cohesive erosion behaviour. Above this threshold, sediment mixtures consolidate in a cohesive way, whereas for smaller clay percentages only weak cohesive behaviour occurs. The settling behaviour of silt-rich sediment is found to be in analogy with granular material at concentration below 150 g/l. Above 150–200 g/l, the material settles in a hindered settling regime where segregation is limited or even prevented. The results indicate that for modelling purposes, multiple sediment fractions need to be assessed in order to produce accurate modelling results.

**Keywords** Yangtze River · Yellow River · Hindered settling · Consolidation · Mixed sediment

---

Responsible Editor: Andrew James Manning

---

This article is part of the Topical Collection on the *11th International Conference on Cohesive Sediment Transport*

---

S. te Slaa · Q. He  
State Key Laboratory of Estuarine and Coastal Research,  
East China Normal University, Shanghai 200062, China

S. te Slaa (✉) · D. S. van Maren · J. C. Winterwerp  
Delft University of Technology,  
Faculty of Civil Engineering and Geosciences, Stevinweg 1,  
2628 CN Delft, The Netherlands  
e-mail: s.teslaa@gmail.com

D. S. van Maren · J. C. Winterwerp  
Deltares, PO Box 177, 2600 MH Delft, The Netherlands

## 1 Introduction

In general, the rate of suspended sediment transport is governed by erosion and sedimentation processes. Sedimentation (net increase in bed level) generally prevails during relatively low-energy conditions, whereas sediment is resuspended from the bed during more energetic conditions. The shear stress at which sediment is eroded depends on the grain size (non-cohesive sediment), or on the degree of consolidation and material properties of clay (cohesive sediment). Cohesive sediments consolidate, thereby increasing their resistance against erosion in time, whereas non-cohesive sediment beds form a rigid bed upon deposition. The erosion threshold of non-cohesive material therefore only depends on grain size, and is reasonably known from Shield's (1936) diagram for the initiation of motion. Van Rijn reports on more recent work (1984; 2007) on transport of non-cohesive material. Erosion processes of mud beds have received attention since the work of Partheniades (1962), Krone (1962) and Ariathurai and Arulandan (1978). The erosion rate of mud beds depends on the degree of consolidation of which our knowledge has advanced significantly since the pioneering work of Terzaghi and Fröhlich (1936), through the work of, e.g. Been and Sills (1981) and Merckelbach (2000). Since the 1990s, more attention has been paid to mixtures of sand and mud. The effect of mud on erosion thresholds of sand–mud mixtures was determined by, e.g. Mitchener and Torfs (1996) and Van Ledden et al. (2004), and of sand on mud beds by Jacobs (2011). Similarly, the impact of sand on hindered settling [Dankers and Winterwerp (2007), Cuthbertson et al. (2008; 2010) and Manning et al. (2011, 2010)] and consolidation (Torfs et al. (1996) are reasonably well understood.

Compared to the present state of knowledge on the behaviour of sand, mud and sand–mud mixtures, little is known about erosion and sedimentation processes of silt-dominated mixtures. Here, silt is defined as the sediment

fraction of which the particle sizes vary between 2 and 63  $\mu\text{m}$  with a base-mineral that does not show cohesive behaviour, e.g. quartz and feldspar. Silt is the most abundant sediment type in China's main rivers; the Yangtze River and the Yellow River. Knowledge on the behaviour of silt is especially important for these rivers. This holds both for sedimentation and erosion processes.

Roberts et al. (1998) demonstrated that the erosion rate of silt particles strongly depends on the density of the silty bed, and that the density of silty beds increased with time as a result of consolidation-like processes. Unfortunately, Roberts et al. paid little attention to this behaviour, which we will refer to as pseudo-consolidation. Moreover, Roberts used industrial instead of natural sediment, without any clay or sand fraction. This makes it difficult to determine to what extent Roberts' results can be applied to natural conditions. Up to now, no dedicated experiments exist on the deposition behaviour of natural silt-dominated sediment mixtures. We therefore set out to do dedicated experiments on the compaction (pseudo-consolidation) and settling behaviour of silt-dominated sediment mixtures.

The aim of this paper is to obtain more fundamental knowledge on the settling and (pseudo-)consolidation of silt-dominated sediments in general. The properties of silt and the relevance for better understanding of erosion and consolidation behaviour are elaborated in Section 2. Our methods are introduced in Section 3, and results presented in Section 4. After discussion (Section 5), we present our conclusions.

## 2 Silt-dominated systems

### 2.1 Definition of silt and silt skeleton

Sediments consist of mineral and organic components. This study restricts to the minerals, in which silicates are predominant. Mineral composition enables to distinguish between these silicates. The main forms of silicates are quartz, feldspar and clay minerals. Minerals encountered in the riverine environment are silicate and phyllo-silicates. Silicate minerals are formed by a framework of silicon-oxygen tetrahedra, described by the overall formula  $\text{SiO}_2$ . Feldspars are a group of rock-forming silicate minerals that make up as much as 60 % of the earth's continental crust. After feldspar, quartz is the most abundant silicate mineral. Phyllo-silicates (sheets) are clay minerals built from tetrahedra structures. Clay minerals can be divided into the following groups; kaolin (China clay), smectite (including montmorillonite), illite and chlorite. The most important difference between phyllo-silicates (clays) and silicates (silts and sands) is that the former can bind water whereas the latter cannot.

Generally, cohesive sediment mixtures consist of clay, silt, (fine) sand particles, organic matter and water. Particle size analyses enable to distinguish individual sediment particles. The three size fractions common in (fine) sediments dynamics are clay, silt and sand. Non-cohesive sediment consists of sand and gravel sized particles ( $d > 63 \mu\text{m}$ ). In the silt fraction ( $2 \mu\text{m} < d < 63 \mu\text{m}$ ) quartz and feldspar are the dominant minerals, whereas in the clay fraction ( $d < 2 \mu\text{m}$ ) kaolinite, illite, smectite (or montmorillonite) and chlorite are dominant. It must be stressed that these categories refer to sediment size classes and not to physical properties, such as cohesiveness. This implies that in the silt fraction clay minerals can be present, and vice versa. Little information can be found in the literature on the behaviour of the silt fraction with respect to its sedimentation and entrainment behaviour. Silt is classified as non-cohesive from a mineralogical point of view, since its main constituents are quartz and feldspar. However, erosion studies on silt-rich sediment indicate cohesive-like behaviour (Jin et al. 2002; Roberts et al. 1998).

When considering the mechanical behaviour of fine sediment-mixtures, the mineral composition in combination with particle size distributions are important discriminators. Ternary diagrams are commonly used to illustrate mass fractions of sand, silt and clay to classify sediment types. The presence of clay minerals is a criterion for sediment mixtures to show cohesive behaviour. Van Ledden et al. (2004) argues that transition in erosion behaviour can be expected when (1) the bed changes from cohesive to non-cohesive and (2) the sediment type determining the governing network changes. Cohesive or non-cohesive behaviour is attributed to the clay content. A transition is found at clay contents of 5–10 %. The network structure depends on the overall porosity. Granular skeletons occur when sand and/or silt particles are in mutual contact. A sand network structure occurs when the volume fraction of sand exceeds 40–50 % (Kuerbis et al. 1988; Floss 1970). Similarly, silt particles form a network structure when the volume fraction of the silt particles ( $\Psi_{\text{si}}$ ) relative to the pore volume around the sand particles [ $\Psi_{\text{si}}/(1 - \Psi_{\text{sa}})$ ] is higher than 40–50 %. In other cases, the clay fraction forms a network structure if sufficient clay is present in the sediment mixture. However, the clay content must be higher than the aforementioned offset in order to form a network structure. Because of the cohesive properties of the clay particles, very open-structured networks can be formed, requiring only a small clay volume fraction relative to the pore fraction left by the silt and sand particles. Sand and silt particles can then be treated as single entities, whereas the volume-filling network is formed by the clay fraction (Merckelbach 2000). The subzones, which classify as soil based on the formed network structure are shown in Fig. 1, where sand- and silt-dominated skeletons are indicated by areas A and B, respectively. This study focuses on sediment in area B.

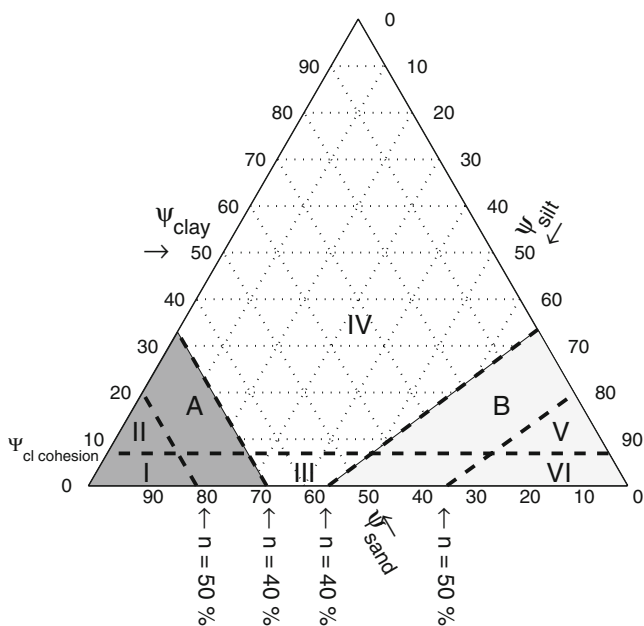


**Fig. 1** Sand–silt–clay triangle with transition for cohesion and network structures.  $\Psi_s$  represents the solid fraction of sand, silt and clay. *I*, non-cohesive sand dominated; *II*, cohesive sand dominated; *III*, non-cohesive mixed; *IV*, cohesive clay dominated; *V*, cohesive silt dominated; *VI*, non-cohesive silt dominated network structure. *Bold broken lines* represent transition to sand or sand–silt-dominated network structures for overall porosities of  $n=40\%$  and  $n=50\%$ . The *horizontal broken line* represents a claycontent (8%) for the transition between cohesive and non-cohesive behaviour. *Shaded areas A and B* indicate the area of sand- and silt-dominated network structures, respectively. Redrawn after Van Ledden et al. (2004)

### 2.2 Implications of silt-rich sediment systems

Both the Yangtze and Yellow River originate at the Qinghai-Tibetan Plateau in Western China from where the Yellow River continuous her course through the Chinese Loess Plateau. In this region, intense soil erosion and weathering occurs. Its geological composition mainly consists of loess, contributing to about 90% of the huge sediment load. The median particle size of this loess varies between 15  $\mu\text{m}$  in the south to 50  $\mu\text{m}$  in the north (Wan and Wang 1994). Because of the Yellow River course through the rich loess soils in the upper regions of the catchment area, relatively large amounts of  $\text{CaCO}_3$  are dissolved in the water resulting in an increased pH value. pH measurements in the Yellow River show values of individual tributaries between 8.2 and 8.7 (He et al. 2006; Wu et al. 2005b; Xia et al. 2004). For the Yangtze River, average pH value of individual tributaries is between 7.7 and 8.4 (Chen et al. 2002). The influences of these relatively high pH values of the Yellow River water on sedimentation processes are yet unknown. The two major sediment-producing areas of the Yangtze River, the drainage areas of the lower Jinshajiang (eastern Qinghai plateau) and the Jialingjiang (central China) rivers, produce 70% of the

river’s total sediment load. The median grain size at the control station of the Jinshajiang River is approximately 20  $\mu\text{m}$ , and at the control station of the Jialingjinag River the sediment fraction coarser than 50  $\mu\text{m}$  is only 8% (Xu 2007). This causes the Yangtze and Yellow Rivers to carry large silt contents in their sediment discharge causing implications in understanding their morphological behaviour. Some implications of silt-rich sediment are addressed below:

- Van Maren (2007; 2009a; 2009b) identifies several hydrodynamic and soil mechanical processes that play a role in the Yellow River, which are attributed to high silt contents. The occurrence of hyper-concentrated flow may lead to a collapse of the turbulent flow field, resulting in massive deposition on the floodplains and in the main channel. Consequently, water is captured in the bed resulting in an excess pore water pressure. Over time, this excess pore water pressure dissipates, thereby decreasing the porosity of the bulk material. As a result, the critical bed shear stress for erosion increases. This process, governed by pore water pressure dissipation rates, is much faster for silty sediment than for clays. The morphological behaviour of the river channel therefore depends on the pseudo-consolidation behaviour of silt.
- Roberts et al. (1998) performed erosion experiments with pure quartz particles, thereby varying the particle size  $d_{50}$  between 5 and 1,350  $\mu\text{m}$ . They found that with increasing particle size, the erosion rate first increases, reaches a maximum, and then decreases. In their experiments, they observed that the bed eroded as chunks. Such mass erosion is an indication for cohesive sediment behaviour. For cohesive sediment, it is known that the time scale of the driving mechanism is a determining factor for the response mechanism of the bed (see Winterwerp and Van Kesteren 2004); when deformation rates are high, pressure gradients will not be compensated by pore water flow. The behaviour of the bed is referred to as undrained erosion and the bed erodes in chunks.
- Over the last 50 years, large reservoirs are being constructed in both river systems, trapping large amounts of silt. As a result, both rivers are becoming sandier, which may strongly alter the dynamic behaviour of sediment. Better knowledge on the behaviour of silt enables a more accurate prediction reservoir siltation.

These observations suggest that the stability/erodibility of silt-rich sediment is governed by the ratio between deformation of the soil and the status of the pore water pressure. The deformation rate of the soil is a function of the eroding forces, the pore water pressure and the dissipation rate of pore water over or under pressure. The rate of dissipation of

pore water pressure gradients is a function of particle size and packing of the silt skeleton. Pore water pressure gradients and packing are governed by the way the bed is formed. To better understand these bed formation processes, laboratory deposition experiments are carried out on silt-rich sediments from both the Yangtze and Yellow River.

### 3 Study area and fieldwork

To better understand the behaviour of silt-dominated sediment in natural systems, fieldwork is carried out at two silt-rich environments in the Yangtze Estuary and the Lower Yellow River (Fig. 2). In both systems, 30-cm-long sediment cores are taken to determine in situ densities and particle size distributions (PSD). Bulk samples were taken to study sedimentation behaviour under confined laboratory conditions. In the Yangtze Estuary, additional surface sediment samples are taken. In order to perform sedimentation

experiments under natural conditions, water samples are also collected in the field. Fieldwork processing and sedimentation experiments are carried out at the State Key Laboratory of Estuarine and Coastal Engineering (SKLEC) of the East China Normal University (Shanghai).

#### 3.1 Study area

##### 3.1.1 Yangtze River estuary

The Yangtze Estuary is shaped by fluvial deposits from the 6418 km long Yangtze River and by tides, resulting in a typical funnel-shaped estuary. The most important morphological features of the Yangtze Estuary are extensive intertidal flats separated by large channels. Upon entering its estuary, the Yangtze River is divided by Chongming Island into the North Branch and the South Branch. Chongming Island is the largest island in this estuary covering approximately 1,600 km<sup>2</sup>. On the East of this island, ecologically important wetlands can be found with

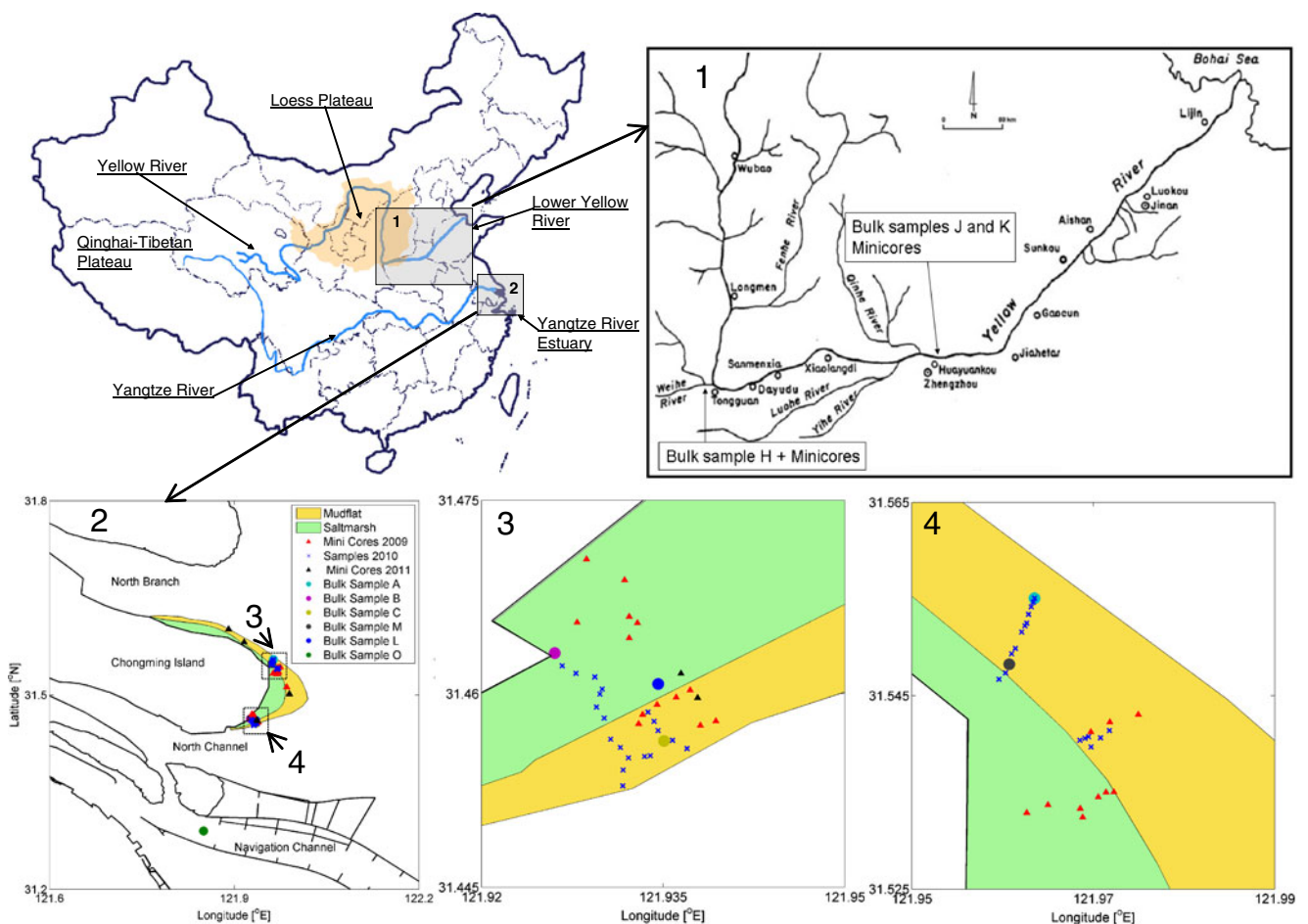


**Fig. 2** The Yangtze River and the Yellow River in China. The Lower Yellow River (1) and the Yangtze River Estuary (2) are sites for fieldwork and sediment sampling in present study. Sampling locations

of minicores, surface and bulk sediment on Chongming Island are indicated in 2, 3 and 4. Yellow River sampling locations for minicores and bulk samples H, J and K are indicated in 1

an area of about 326 km<sup>2</sup>. These wetlands consist of an unvegetated tidal flat and a vegetated salt marsh. This tidal flat is the source of all Yangtze Estuary samples. For simplicity, we will refer to the sediment from this location as Yangtze Estuary sediment.

### 3.1.2 Lower Yellow River

The Yellow River is characterized by extremely high sediment loads and deposition rates, and rapid channel migration (Wu et al. 2005a). This rapid morphological development is attributed to high loads of dominantly silty sediment. Samples were taken in the braided reach of the Yellow River and its main tributary (the Weihe River, just upstream of its confluence with the Yellow River).

### 3.2 Fieldwork and processing

Fieldwork is carried out in late September 2009, early November 2010 and late April 2011 in the Yangtze Estuary, and in April 2011 in the Lower Yellow River. During the fieldwork mini-cores, surface samples and bulk samples are taken. Sampling methods and times of sampling are shown in Table 1. Yangtze Estuary sampling locations of mini-cores, surface sediment (upper 3 cm) and bulk material (sample of several kg) are shown in Fig. 2 (2, 3 and 4). Sampling has been done both on the tidal flats and in the marsh. One bulk sample was taken from the navigation channel (sample O).

In the Lower Yellow River, mini-cores and bulk samples are sampled near Huayuankou (unvegetated floodplain; samples J and K) and from the Weihe River (unvegetated river bank; sample H), close to where it meets the Yellow River, see Fig. 2 (1).

Mini-cores were taken by using 30-cm-long PVC pipes with an inner diameter of 36 mm and sharpened edges at the intruding side. A plunger (from a 100-ml syringe) of equal diameter fits inside the PVC pipe. To reduce compaction of the sediment during extraction, the plunger was held at the sediment surface while the PVC pipe was pushed into the sediment. This method has been applied previously by Montserrat et al. (2009). After sampling, the cores were

frozen. The time between sampling and freezing varied between 5 to 48 h. Next, the cores were sliced into intervals ranging from 2 to 7 cm. These intervals were analysed on porosity and PSD. Surface sediment samples (upper 3 cm) are only analysed on PSD. Bulk sediment samples were taken in combination with water samples, to be used in the laboratory experiments; bulk samples remained constantly saturated.

PSD analysis of surface samples and mini-cores was done by making use of laser diffraction (LS-100 particle size analyzer). All samples were dispersed chemically by treatment with a sodium–hexametaphosphate solution, in combination with ultrasonic dispersion.

### 3.3 In situ conditions and spatial segregation

Yangtze Estuary sediment shows a variety of sediment compositions as a result of spatial variations (Fig. 3). According to the classification by Van Ledden et al. (2004), these sediments can be classified as cohesive silt, non-cohesive silt and non-cohesive mixed (areas V, VI and III in Fig. 1, respectively). Chongming Island tidal flat sediment is found to be mainly silt dominated, where the southern-eastern tidal flat is governed by non-cohesive silt and non-cohesive mixed in contrast to the silt-dominated north-eastern tidal flat. The porosity isolines in Fig. 3 indicate the boundaries of sand or silt-dominated network structures for different porosities (Van Ledden et al. 2004). Maximum porosities correspond with the loosest packing of a granular skeleton and is approximately 50 %, whereas minimum porosities correspond to the most dense packing of a

**Table 1** Timetable of fieldwork activities in the Yangtze River Estuary and the Lower Yellow River

	Sept 2009	Nov 2010	April 2011
Yangtze Estuary	Minicores	Surface samples A, B and C	Bulk samples L, M and O
Yellow River	–	–	Minicores Bulk samples H, J and K

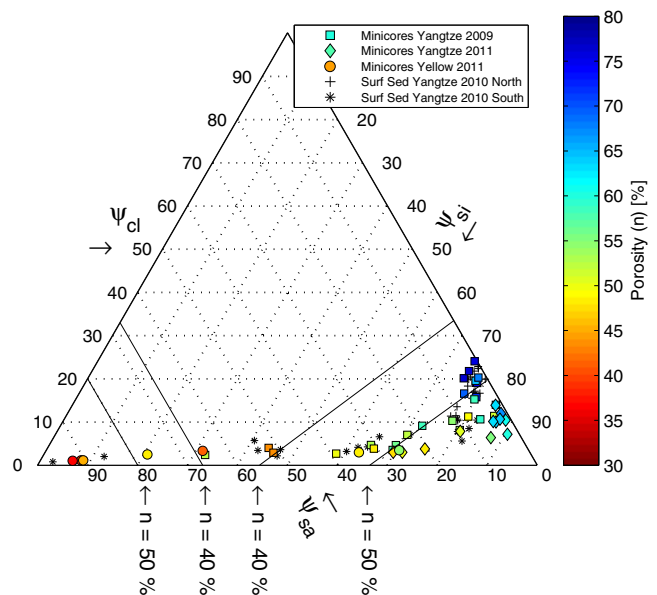


**Fig. 3** Ternary diagram of sand–silt–clay distributions in Yangtze Estuary and Yellow River 2009 and 2011 minicores in combination with measured in situ porosity and Yangtze Estuary surface sediment samples

granular skeleton which is approximately 40 %. The in situ porosities of the upper 30 cm of Yangtze Estuary sediment generally varies between 40 and 80 % and is especially high for  $\psi_{cl} > 10$  %. Below this threshold, in situ porosities are approximately 10 % larger than the porosity isolines in the silt-dominated area, whereas above this threshold in situ porosities are up to 50–60 % larger. In addition, clay/silt ratios of approximately 0.125 are observed for  $\psi_{sa} > 5$  %, whereas for  $\psi_{sa} < 5$  % clay/silt ratios vary between 0.38 and 0.1.

Sediment from the Yellow River floodplains is found to be non-cohesive, varying between sand-dominated, silt-dominated and a mixture of these types (areas I, III and VI in Fig. 1). Clay contents do not exceed 6 %. Again, in situ porosities deviate only 5 % from the porosity isolines in the sand-dominated area. Sediment porosities do not exceed 50 %. In general, a trend of decreasing in situ porosity is observed with increasing sand content, following porosity isolines. Porosities below 45 % are only rarely observed, which is expected as the minimum possible porosity is approximately 40 %.

#### 4 Sedimentation experiments

Consolidation processes are usually studied using settling columns, primarily focusing on density development within the consolidating bed itself, and excess pore water pressure dissipation. In previous studies, pore water pressure measurements were done with piston riser tubes or pressure transducers. Here, pore water pressure is measured using pressure transducers. In previous studies (Been and Sills 1981; Merckelbach 2000) density profiles were measured by making use of X- or  $\gamma$ -radiation. A great advantage of this method is that it is non-intrusive and measures a continuous vertical profile with high accuracy ( $\pm 2 \text{ kg/m}^3$ ). However, the extensive safety measures required with respect to radiation hazards make this method increasingly difficult to apply. Therefore, we use a new method in our sedimentation experiments, which uses electrical conductivity to measure densities. The greatest advantage of this method is that it allows measuring a continuous density profile during the sedimentation experiment. Other advantages are the non-intrusiveness without the disadvantage of radiation hazards. A disadvantage is the large influence of temperature fluctuations, which needs to be compensated from continuous temperature measurements.

Below, we will first introduce the settling column set-up, followed by calibration and measurement protocols.

##### 4.1 Set up settling columns

All sedimentation experiments are carried out in 1.30-m-high PMMA transparent columns. The inner diameter of

these columns is 10.0 cm. The columns are equipped with an impermeably base. A scale bar attached to the column wall enables the measurement of interface development. Pore water pressure ports are mounted in the column walls at ten intervals of 5.0 cm each, starting at 5.0 cm from the bottom. In addition, one port is located at a level of 1.0-m height, which is used as a reference pressure, since it is always located above the sediment. Each port entry was provided with a Vyon plastic filter to prevent sediment leaks. The ports were connected via small tubes to a pressure-measuring unit. This method has been previously used by Bowden (1988) and later by Merckelbach (2000). The pressure-measuring unit houses one pressure transducer. This pressure transducer can be connected to any of the pressure ports, one at a time. The transducer is connected to a variable water head for calibration. The accuracy of the pore water pressure values from calibration is 1-mm water head, or 10 Pa.

The density parameters are measured using electrical conductivity. This is done with a conductivity concentration meter (CCM) developed by Deltares. The principle of a CCM measurement is based on the conductivity gradient of a sediment–water mixture due to a gradient in non-conductive sediment concentration in the monitored area. The CCM houses 20 ports, which can measure simultaneously. Each port is connected to a double platinum electrode, mounted in the wall of the column, flush with its curvature to reduce the influence of the probes on the deposition process. Each pair of electrode is placed with a mutual vertical distance of approximately 1 cm. The vertical placement differs from the method used by Blewett et al. (2001), where the electrodes were placed opposite of each other along the column wall. We will refer to a pair of electrodes as a (conductivity) probe. All columns houses 10 of these conductivity probes at 5, 15, 20, 25, 30, 35, 40, 45, 50 and 65 cm from the base plate. The top probe was placed at a higher level with the aim to function as a reference measurement in the overlying clear water. In total, five columns (with 10 conductivity probes each) are available for our experiment and therefore not all experimental series can be carried out simultaneously. A new series of experiments within the same columns requires re-calibration of all 10 conductivity probes.

The setup was placed in an air-conditioned environment, but nonetheless not free from temperature fluctuations. In order to correct for temperature fluctuations, the temperature inside the columns is measured at the tip of a 50-cm-long temperature probe. The sensitivity of the temperature probes has a resolution of  $\pm 0.1$  °C. Temperature and conductivity measurements inside a single column are always carried out simultaneously.

## 4.2 Conductivity probes

### 4.2.1 Theory of conductivity measurements

Electrical conductivity of a medium is sensitive to temperature, salinity, pH and solid content fluctuations. In this study, pH and salinity are constant in all experimental series; hence, our conductivity measurements are a function of temperature and solid content. The electrical conductivity as function of water is generally non-linear. However, the degree of nonlinearity is relatively small in a temperature range of environmental monitoring (0–30 °C) and a linear equation is commonly used to represent this relation (Sorensen and Glass 1987). In our study, the temperature is generally kept between 20 and 25 °C. Therefore, the conductivity of water and the sediment–water mixture can be described by:

$$\begin{aligned} K_w &= K_{w,\text{ref}}(1 + \kappa\Delta T) \\ K_m &= K_{m,\text{ref}}(1 + \lambda\Delta T) \end{aligned} \quad (1)$$

Where  $K_w$  and  $K_m$  are the conductivity of water and the sediment–water mixture respectively,  $K_{w,\text{ref}}$  and  $K_{m,\text{ref}}$  are reference conductivities,  $\Delta T$  a temperature gradient and  $\kappa$  and  $\lambda$  coefficients describing the influence of temperature on conductivity. Dai et al. (2009) studied the relationship between suspended sediment concentration and electrical conductivity. A linear relation between sediment concentration and electrical conductivity was found, which can be written as:

$$\phi_s = \left(1 - \frac{K_m}{K_w}\right)a \quad (2)$$

Where  $\phi_s$  is the volume concentration (defined as the ratio of solids volume and the total wet volume) and  $a$  represent the conductivity parameter. From  $\phi_s$ , the mass concentration  $c$  is computed via  $c = \rho_s \phi_s$ . Substituting (1) in (2) results in a function describing the solid content as a function of temperature, solid content and electrical conductivity.

### 4.2.2 Calibration and accuracy

In each column, a series of sedimentation experiments is carried out with sediment from different sources (see Section 3.3 for a detailed explanation). All probes in each column are calibrated with the same sediment–water mixture as used in the corresponding series of sedimentation experiment. By rewriting (1) and (2) as

a polynomial function the measured concentration can be expressed in terms of  $\phi_s$ :

$$V = \alpha T + \beta\phi_s + \gamma T\phi_s + \varepsilon \rightarrow \phi_s = \frac{V - \alpha T - \varepsilon}{\beta + \gamma T} \quad (3)$$

Where  $V$  is the output voltage of a conductivity measurement,  $T$  the temperature,  $\phi_s$  the solid content and  $\alpha$ ,  $\beta$ ,  $\gamma$ , and  $\varepsilon$  are coefficients. In this way, the linear influence of temperature, the linear influence of solid fraction and one cross term for the influence of temperature and solid fraction are taken into account. For our experiments, coefficients  $\alpha$ ,  $\beta$ ,  $\gamma$ , and  $\varepsilon$  are determined by calibration. Therefore, a calibration is carried out both on concentration and temperature. In a specially designed calibration beaker samples are prepared of which the output voltage of the CCM is measured for different temperatures, the latter one is increased by using an immersion heater. The measurement error of each probe system (temperature, probe distance, wiring) is defined as the root mean square error (RMSE,  $\sigma_\varepsilon^2$ ) of measured ( $M$ ) and observed concentration ( $O$ ) for each temperature–concentration combination ( $i$ ). In addition, the RMSE was determined for each individual concentration, for which a characteristic (for all columns) result of column L is shown in Fig. 4. The RMSE ( $\sigma_\varepsilon^2$ ) is defined as:

$$\sigma_\varepsilon^2 = \sqrt{\frac{\sum (M_i - O_i)^2}{n}} \quad (4)$$

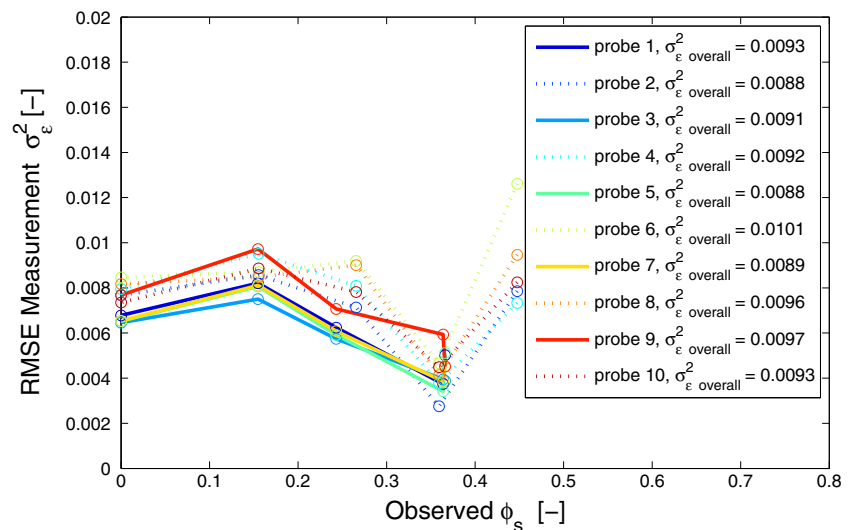
Since the RMSE varies only little over the range of observed  $\phi_s$ , the accuracy of each probe is defined as the overall RMSE of the calibration. For all probes in each column, the accuracy in  $\phi_s$  is found to be below 0.01, corresponding with a mean error in concentration smaller than  $\pm 26.5$  g/l.

Segregation occurred in most of our experiments, resulting in a vertical variation in sediment composition. Due to an anticipated different conductivity per composition, calibrations were carried out with the sandiest and the most clayey composites. Surprisingly, we found that there was no measurable difference in electrical conductivity between these for our experiments extreme composites. The variation in clay content of approximately 8 % is apparently not influential enough to result in significant changes in conductivity in present measurements.

### 4.3 Experimental method and program

A total of nine bulk samples are collected from the field; six from the Yangtze River Estuary and three from the Yellow River floodplains (Fig. 2). The Yangtze River bulk samples are labelled A, B, C, L, M and O and the Yellow River bulk samples are labelled H, J and K. With each of these bulk samples a series of sedimentation experiments are carried

**Fig. 4** Calibration errors for all probes in column L. Overall RMSE's for each probe are depicted in the legend.



out in different settling columns, one column for each sample, labelled with a letter referring to the bulk sample. For each new experimental series, the conductivity probes need to be re-calibrated since the conductivity of the pore water changes per sampling location. All columns are equally equipped with measurement devices. In all experimental series, the initial concentration varies for each experiment. During sedimentation, vertical mass concentration and vertical pore water pressure profiles are measured. In addition, visual interfaces are recorded manually.

All nine series of sedimentation are carried out following the same protocol. For each experimental series, a container was prepared with sufficient sediment and water to fill a column with initial concentrations of up to 800 g/l. To achieve this, the bulk samples had to be diluted. For columns A, B, C and O, water at the proper pore water salinity was added. Water added to the sediment for columns H, J, K, L and M originated from the corresponding sampling location. The overlying clear water in each container is introduced into the column first. With this clear water, a reference concentration measurement is carried out, and the tubes leading to the pressure transducer are carefully filled with water to prevent air-entrapment within. Next, the sediment within the container is homogeneously mixed again for 5 min after which a volume of the sediment–water mixtures from the container was added to the column. Now, the sediment–water mixture within the column is mixed gently with a porous pouncer for 5 min after which the mixture is left to settle. For each following test with higher initial concentration in the same series, the container was mixed up again and a new volume from the container was added to the column. The initial concentrations were obtained by averaging the measured concentration during the first 10 s of each test. During the experimental series, the container and the columns are sealed to prevent evaporation of the pore water. Calibration of the conductivity probes is carried

out after each experimental series. In this way, it can be checked whether any drift of the probes had occurred with respect to the initial clear water concentration measurement.

Table 2 presents all initial concentrations used in all series. It can be seen that the smallest initial concentrations are in the same order of magnitude as the accuracy of the conductivity probes. Since settling velocities are relatively large at these concentrations, both the clear water concentration and the concentration during settling are measured within the same timescale. The offset from the clear water concentration is a certainty and therefore quantitative measurements at the low concentrations are still considered usable. Only during the last experiment, pore water pressures are measured. After the last experiment, sediment samples are taken along the columns. This is done at the locations of the conductivity probes.

Due to blurring of the conductivity signal during measurements in columns M and O, only visual observations of the sediment–water interface are recorded. The reasons for the failure of these conductivity measurements can be multiple, but has not been subject of study in this research.

## 5 Sedimentation experiments: results and analysis

The bulk samples reflect the spatial variation in sediment composition, following from PSD analysis (Fig. 5) and corresponding sand, silt, clay contents and  $d_{50}$  (Table 3). A series of sedimentation experiments is carried out with these samples, as described in Section 3. Before analyzing our results, we will describe measurement results and analysis of one settling column sedimentation experiment in detail (Fig. 6: experiment A10).

In the majority of the experiments (including A10, Fig. 6) segregation is observed visually, resulting in two interfaces. An upper interface represents the top of a settling clay–water



**Table 2** Initial concentration in experimental series in g/l. T1–T12 represents the number of experiments per series

	Test number											
Series	1	2	3	4	5	6	7	8	9	10	11	12
<b>A</b> Yangtze	–	–	82	175	155	224	281	314	252	382	426	<b>396</b>
<b>B</b> Yangtze	41	44	144	154	209	218	213	<b>401</b>	–	–	–	–
<b>C</b> Yangtze	66	160	241	290	<b>367</b>	–	–	–	–	–	–	–
<b>H</b> Yellow	76	278	205	298	334	414	<b>667</b>	–	–	–	–	–
<b>J</b> Yellow	11	74	131	249	310	<b>488</b>	–	–	–	–	–	–
<b>K</b> Yellow	42	143	119	135	<b>364</b>	–	–	–	–	–	–	–
<b>L</b> Yangtze	545	717	705	701	720	<b>707</b>	–	–	–	–	–	–
<b>M</b> Yangtze	40	56	75	104	<b>343</b>	–	–	–	–	–	–	–
<b>O</b> Yangtze	24	44	62	78	<b>211</b>	–	–	–	–	–	–	–

Results of bold marked initial concentrations are visualized in Fig. 10

mixture. A clear transition between this layer and the overlying clear water indicates that all particles settle at a single velocity. Sediment in this layer consists of a clay–water mixture as revealed by particle size analysis, and the observation of drainage channels [resulting from non-homogeneously distributed fluid flow in the horizontal plane, characteristic for clay-dominated mixtures (Winterwerp and Van Kesteren 2004)] Initially, the upper interface settles with a constant velocity until time  $t_3$ . Here, an inflection point in the settling curve is observed. From this point forward, the settling velocity is reduced significantly indicating the transition from a hindered settling regime into consolidation beyond time  $t_3$ . Hence, this inflection point represents the gelling point (Dankers 2006). A second, internal interface marks the transition between the settling and/or consolidating clay–water mixture and underlying granular layer. This granular layer builds up

between times  $t_0$  and  $t_2$ , indicating that the majority of the granular material settles within this timeframe.

Concentration isolines (isolutes) are derived from the continuous concentration measurements. These isolutes initially increase linearly in time (until inbetween  $t_1$  and  $t_2$ ) in the lower 27 cm and decrease linearly in time (until  $t_1$ ) in the overlying mixture. After  $t_2$  the isolutes in the lower 27 cm are horizontal. The first derivative of these isolutes provides a settling velocity within the settling sediment–water mixture (internal settling interface). Between  $t_1$  and  $t_2$ , the isolutes converge, indicating an increasing vertical concentration gradient, and hence a reduction in settling velocity. After  $t_2$ , the isolutes in the lower 27 cm are horizontal, marking complete sediment deposition.

In addition to interface observations and concentration measurements, a pressure transducer measures pore water pressures to determine excess pore water pressure dissipation. At the end of each experiment ( $t_{end}$ ), sediment was collected from the settling column at the locations of conductivity probes (which are removable) for particle size analysis.

Summarizing, the experiments consist of a phase with rapid settling of granular material, allowing computation of

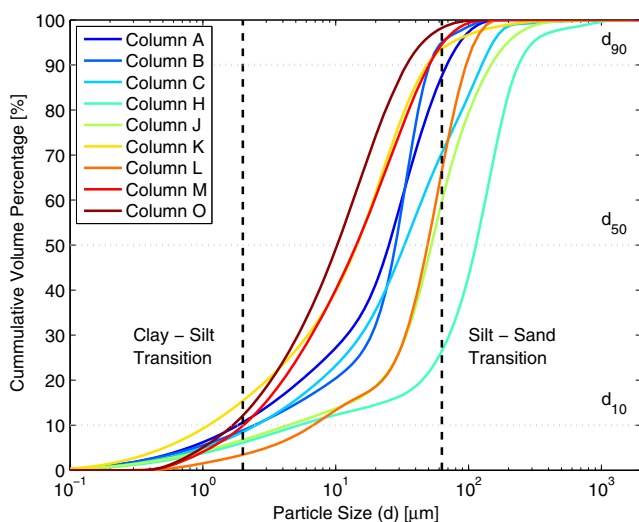


**Fig. 5** Grain size distribution of material used in settling column experiments. Black dotted lines indicate clay–silt (2 μm) and silt–sand (63 μm) transitions

**Table 3** Sand, silt and clay contents, and  $d_{50}$ 's of sediment used in column experiments

Column	Cl [%]	Si [%]	Sa [%]	$d_{50}$ [μm]
A Yangtze	11	77	12	25
B Yangtze	9	86	5	28
C Yangtze	8	62	30	33
H Yellow	6	20	74	114
J Yellow	7	53	40	53
K Yellow	15	78	7	14
L Yangtze	3	63	34	49
M Yangtze	10	85	5	14
O Yangtze	12	86	2	10

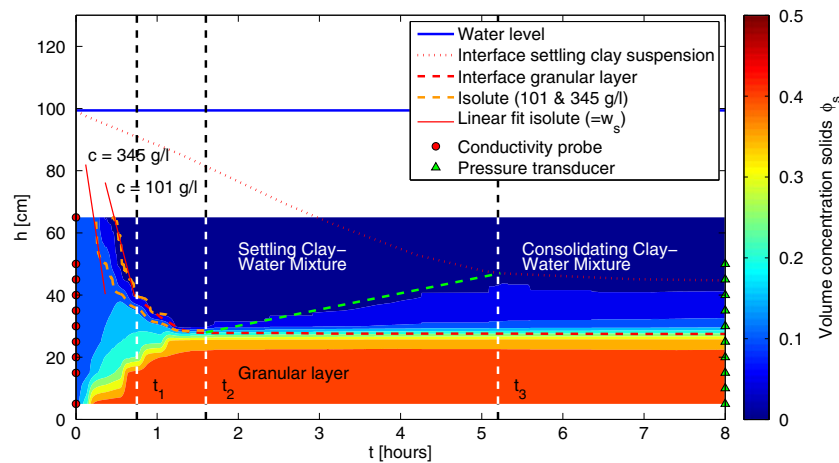


**Fig. 6** Measurement results for the vertical volume concentration profile over time in experiment A10. Visual interface observations are indicated by red dashed lines. Measured  $\phi_s$  isolines between  $t_0$  and  $t_1$  are given for  $c=101$  and  $345$  g/l.  $t_2$  represents the moment where all granular material is settled.  $t_3$  represents the gelling point of the

overlying clay–water mixture. Locations of conductivity probes and pressure transducers are indicated by red dots and green triangles, respectively. The green dashed line indicates a rising internal interface of deposited flocculated material. The concentration along this line equals the gelling concentration

settling velocities ( $t_0-t_1$ ), a phase with settling clays and hindered settling of granular material ( $t_1-t_2$ ), a phase with settling clays in a consolidating bed ( $t_2-t_3$ ), whereas the final stage is a consolidating clay–water mixture ( $t_3-t_{\text{end}}$ ). These measurements allow quantitative analyses of segregation mechanisms, hindered settling velocities and structural densities of multiple sediment fractions, of which results are presented in the next section.

### 5.1 Segregation

Vertical profiles in sediment fraction,  $d_{50}$  and concentration at  $t_2$ ,  $t_3$  and  $t_{\text{end}}$  of the test with the highest initial concentration per series, are shown in Fig. 7 (for some restrictions see Section 3.3). Results for Yangtze Estuary and Yellow River sediment are separately discussed below. Below, we will only refer to the letter of the discussed column(s) in Fig. 7.

#### 5.1.1 Yangtze River estuary sediment (Columns A, B, C, L, M and O)

The largest segregation is observed in column C, which contains together with column L the coarsest sediment of all Yangtze Estuary samples. In column L however, segregation does not occur. In columns A and B, the silt fraction settles from the overlying layer in which clay percentages are higher. In contrast to column C, columns A, B and L show less segregation within the granular layer. The granular layer in column A even shows a more or less constant sand content, only slightly increasing toward the bottom.

Sand is absent in all top layers of columns A, B, C and L indicating that sand and/or silt particles are not supported by

a network structure in the settling phase. The clay/silt ratio in the overlying settling mixture is approximately 0.25 in all these columns whereas the average clay/silt ratio of the bulk sample is 0.14. A constant clay/silt ratio is not observed in the bed. Clay percentage generally decreases with depth, which is compensated by an increasing sand and/or silt content.

The density profiles in columns K (at  $t_3$ ) and L have a sawtooth-like character which is probably caused by local accumulation of pore fluid pockets rather than by a lack of accuracy. We support this suggestion by the measurements in column K, where the sawtooth-like character develops over time.

In columns M and O limited segregation occurred even though initial concentrations are quite low (343 and 211 g/l) in comparison to columns A, B, C and L (367 to 707 g/l). Apparently, the initial concentrations are above the structural density, so a network structure of flocs is formed, reducing the settling velocity of silt and sand particles within the mixture. This can be attributed to the relatively high clay percentages.

#### 5.1.2 Yellow River sediment (Columns H, J and K)

Segregation in Yellow River columns is in analogy with Yangtze Estuary columns; larger particles settle faster, leaving a clay-dominated mixture to settle and consolidate on top of the deposited sand and/or silt-dominated bed. Column H shows constant sand, silt and clay contents in the lower 40 cm of the granular layer, whereas the  $d_{50}$  and  $\phi_s$  clearly decrease in upward direction. In column H, the  $d_{50}$  is primarily determined by the sand fraction (74 %, see Table 3), and therefore the sand–silt–clay segregation does not necessarily relate to the  $d_{50}$ . The clay-dominated mixture overlying the granular layer is relatively thin, because of the low clay content (6 %; see Table 3). In column J, the clay content is

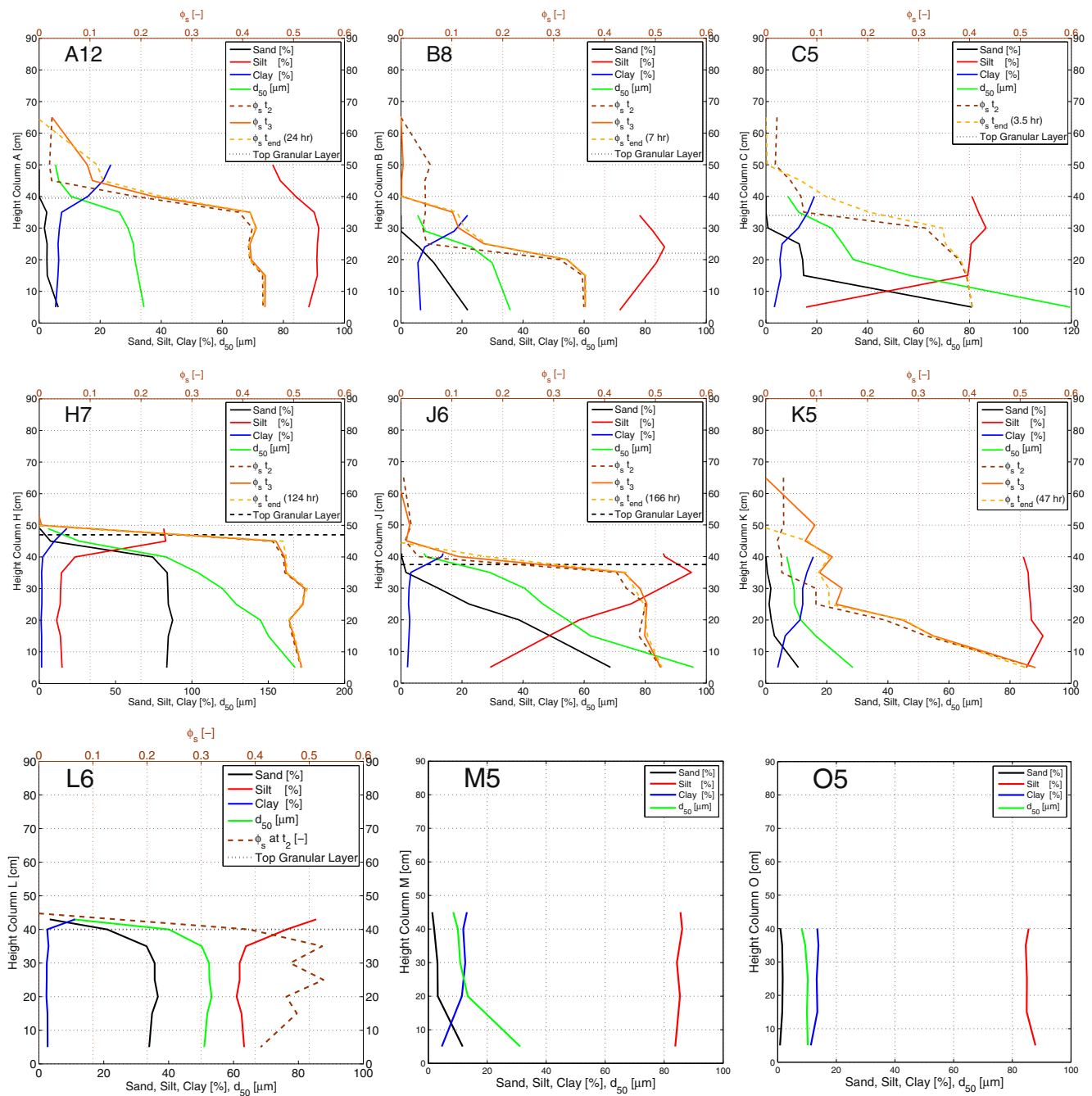


**Fig. 7** Vertical sand, silt, clay and  $d_{50}$  profiles at the end of each compaction/consolidation test for experiments (from top left to bottom right) A12, B8, C5, H7, J6, K5, L6, M5 and O5. Presented GSD's result from direct sampling. These results refer to the tests with the highest initial concentration in each test series. In tests K5, M5 and O5, no

granular layer was observed. Solid contents at  $t_2$ ,  $t_3$  and  $t_{end}$  are indicated with brownish colours. A12 is representative for Fig. 9, but with different initial concentration (338 vs 396 g/l—see Table 1). Note the deviating limits of the x-axis in C5 and H7

also low, and vertically uniform in the granular layer. The sand content increases with depth and  $\phi_s$  increases slightly with the sand content whereas the clay content is constant. Column K shows larger vertically increasing clay contents which results in a more pronounced vertical gradient in solid content  $\phi_s$ . In the lower 20 cm of column K, segregation is the strongest.

### 5.2 Structural density and gelling concentration

The structural density ( $\rho_{str}$ ) of granular material is defined as the concentration at which a space-filling network occurs where particles support each other at their loosest packing. For cohesive (floculated) material the structural density is

defined as the gelling concentration ( $c_{gel}$ ) at which a space filling network develops, which is the onset for consolidation (Winterwerp 2001). When discussing the structural density, we will refer to granular material, whereas we use the term gelling concentration for clay-dominated mixtures. Generally, structural densities are in the order of 1,600–1,800 g/l, whereas gelling concentrations may be as low as 50–100 g/l. In our experiments, both conditions are observed, often simultaneously. Between  $t_0$  and  $t_2$ , granular material forms a network structure, whereas the overlying clay mixture forms a network structure between times  $t_0$  and  $t_3$ .

5.2.1 Structural density

Conductivity probes measure the concentration development during deposition and hence can be used to determine structural densities. The structural density is related to the sediment composition, based on particle size analysis. Most of the sediment samples in the vertical profile of the columns are silt dominated (Fig. 8). The samples without sand (upper layers) have a relatively high porosity. The porosity decreases with increasing sand content (up to  $\Psi_{sa} \approx 20\%$ ); for higher sand contents, the porosity is more or less constant around 50%. An opposite trend is found for the clay content. It is important to note that such a direct correlation cannot be observed for the silt fraction. In the silt-dominated area ( $\Psi_{si} > 67\%$ ), both high and low porosities are found, depending on the fractions of the other two constituents. Sediment mixtures with the largest porosity ( $n > 70\%$ ) do not contain sand and are all located in the overlying

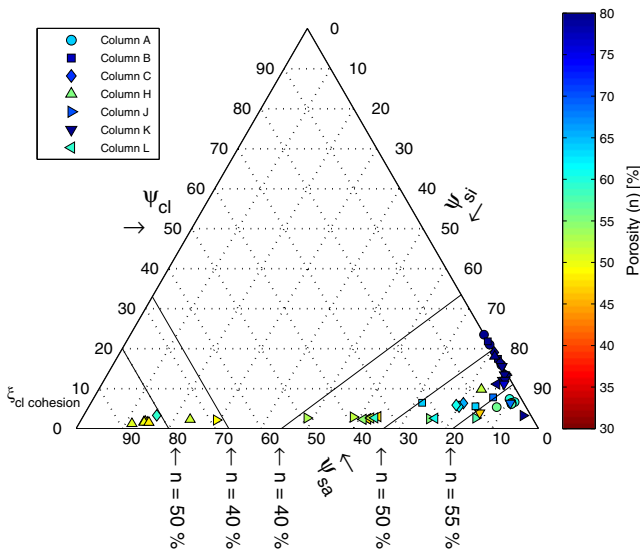


Fig. 8 Ternary diagram of sand-silt and clay content combined with measured porosity ( $n$ ) at  $t_{end}$  in all consolidation/compaction experiments

consolidating sediment layer. These high porosities appear to occur when the clay content exceeds 11%.

Relating  $d_{50}$  to porosity is not straightforward in a ternary diagram, and is therefore plotted against porosity (Fig. 9). The porosity decreases with the median grain size  $d_{50}$ : this can be quantified with a simple empirical formulation by Van Rijn (2007), relating  $\rho_{str}$  and/or  $c_{gel}$  to  $d_{50}$  (median diameter of entire sediment mixture):

$$c_{gel} \text{ or } \rho_{struct} = \frac{d_{50}}{d_{sand}} \rho_{struct,sa} \tag{5}$$

Where  $d_{sand}$  ( $=63 \mu\text{m}$ ) is the smallest particle size of a non-cohesive bed (sand) and  $\rho_{struct,sa}$  is the dry bulk density of the corresponding sand bed;  $\rho_{dry} = (1-n)\rho_s$ . Despite its empirical background, a prediction of porosity, using Eq. (5) shows qualitative similarity with a linear fit through the measured porosities and the  $d_{50}$  for  $d_{50} < 63 \mu\text{m}$ . The gelling concentration of the overlying clay-water mixtures (red dots) are computed using this method as well. Results are presented in Table 7.

5.2.2 Gelling concentration

The gelling concentration of the overlying clay-water mixture can be determined by three other methods: the first

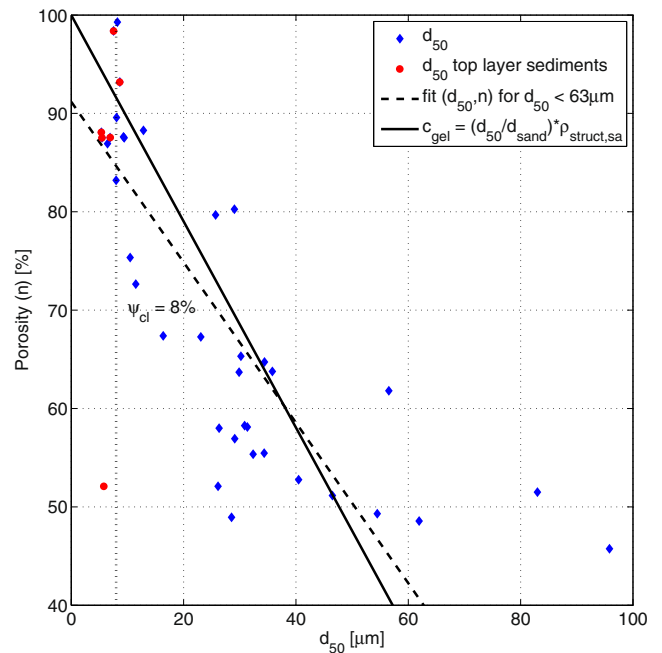


Fig. 9 Porosity as function  $d_{50}$  at  $t_{end}$  in columns A, B, C, H, J and K. The black dashed is a linear fit on the  $d_{50} - n$  data. The black solid line represents Eq. 5. Red dots represent the  $d_{50}$  measured in the top layer of the columns. The vertical dotted line indicates threshold clay content (8%) for cohesive behaviour (Van Ledden et al. 2004)

**Table 4** Gelling concentrations in gramme per litre resulting from direct concentration measurement

	Test number									
Series	2	3	4	5	6	7	8	10	11	12
A Yangtze	–	–	–	–	95	85	115	136	120	140
B Yangtze	–	–	–	94	122	93 <sup>a</sup>	–	–	–	–
C Yangtze	71	80	127 <sup>a</sup>	119	–	–	–	–	–	–
H Yellow	–	–	–	74	45 <sup>a</sup>	78	–	–	–	–
J Yellow	–	–	–	90	101	–	–	–	–	–
K Yellow	–	95	84	80 <sup>b</sup>	–	–	–	–	–	–

<sup>a</sup> Clay suspension settled along interface during deposition of clay–water mixture

<sup>b</sup> Concentration in which segregation is prevented, measured in the settling phase (=minimal  $c_{gel}$ ).  $c_{gel}$  Yangtze River clay=107±22 g/l.  $c_{gel}$  Yellow River clay=81±17 g/l

method by direct measurement (results in Table 4) on the basis of the mass balance of the clay–water mixture by taking the average concentration above and below the internal rising interface of the clay-dominated mixture. This interface is represented by the green dotted line in Fig. 6 (results in Table 5) using settling velocity and concentration measurements. All methods are described extensively by Dankers (2006) in which she argues that the second method overestimates the calculated gelling concentration in comparison with method one. The second method can only be applied for non-granular sediment, which makes it suitable for our results from columns M and O (Yangtze Estuary sediment only). The third method is a result of the research by Dankers, which will be discussed in Section 5.3.

Continuous concentration measurements (method one) during the sedimentation process allow direct determination of the gelling concentration of the overlying clay mixture. For this purpose, a conductivity probe is located within the consolidating layer. Probe 4 of experiment A10 is located within this layer (Fig. 10). The granular material settles from the mixture first, resulting in a concentration decrease in the top four probes and concentration increase in the bottom six probes. Probes where the sediment–water interface settles below, measure zero concentration (clear water). The

concentration measured within the settling mixture start to increase as the flocs settle on the granular bed. Initially, the concentration increases rapidly (settling) after which this increase reduces (consolidation). The transition between the rapid concentration increase and the following reduction is considered to be the gelling point. The corresponding gelling concentrations measured with this method are shown in Table 4 for the experiments in columns A, B, C, H, J and K. Since the thickness of the clay-dominated layers in the consolidation phase of the Yellow River columns is small, only a few direct measurements of the gelling concentration are available.

From our experiments, we have derived a mean gelling concentration of 107±22 g/l using the first and 136±22 g/l using the second method for Yangtze Estuary clay–water mixtures. For Yellow River clay, only the former method is applied for which we derived a gelling concentration of 81±17 g/l.

### 5.3 Settling velocity

As explained in the introduction of this section, settling velocities of both sediment fractions are measured. The first time-derivative of the observed settling interface between  $t_0$

**Table 5** Characteristics of experiment in columns M and O; initial concentration, effective settling velocity, gelling concentration, fractal dimension and permeability parameter

Column+test no.	$c_o$ [kg/m <sup>3</sup> ]	$w_s$ [mm/s]	$c_{gel}$ [kg/m <sup>3</sup> ]	$n_f$ [–]	$K_k$ [m/s]
O1	24	0.18	173	2.69	1.05e <sup>-15</sup>
O2	44	0.12	159	2.72	1.04e <sup>-15</sup>
O3	62	0.09	132	2.74	1.11e <sup>-15</sup>
O4	78	0.06	128	2.75	1.08e <sup>-15</sup>
O5	211	0.004	$c_o > c_{gel}$	2.82	1.34e <sup>-13</sup>
M1	40	0.30	107	2.71	1.05e <sup>-15</sup>
M2	56	0.18	126	2.73	1.07e <sup>-15</sup>
M3	75	0.12	144	2.75	1.11e <sup>-15</sup>
M4	104	0.09	118	2.76	1.11e <sup>-15</sup>
M5	343	0.003	$c_o > c_{gel}$	2.74	8.32e <sup>-13</sup>

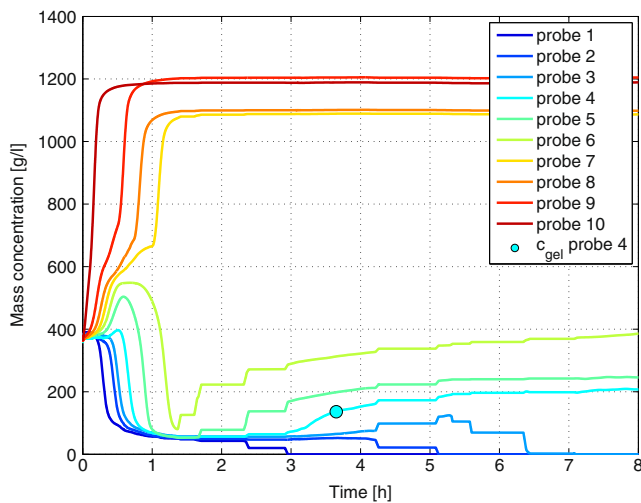


**Fig. 10** Concentration time series for all probes in experiment A10. Probe 1 is at 65 cm from the base of the settling column. Probe 4 is located within the settling and consolidating clay–water mixture and measures a  $c_{gel}$  of 136 g/l at  $t=3.65$  h. Around  $t=5.5$  h the consolidating layer drops below probe 3. Discontinuities are the result of non-continuous measurement

and  $t_3$  gives the effective settling velocities of the clay mixture, whereas the first time-derivatives of between  $t_0$  and  $t_1$  computed isolutes (example in Fig. 6), give the settling velocities of the granular fraction.

### 5.3.1 Hindered settling of clay–water mixtures

Figure 11 shows the effective settling velocities  $w_s$  of the visually observed interface of the overlying clay–water mixture, as function of the measured mass concentration  $\phi_{s,s}$  for Yangtze Estuary sediment (a) and Yellow River sediment (b). The settling velocity decreases with increasing concentration, indicating hindered settling effects. The overlying sediment–water mixture is a clay-dominated mixture for which Dankers (2006) relates the settling velocities to sediment concentration:

$$w_s = w_{s,0} \frac{(1 - \phi)^m (1 - \phi_p)}{1 + 2.5\phi} \quad (6)$$

Where  $w_s$  is the effective settling velocity,  $w_{s,0}$  the settling velocity of individual aggregates,  $\phi_p$  is the volumetric concentration of the primary particles,  $\phi_p = c/\rho_s$  in which  $c$  is the mass concentration and  $\rho_s$  the density of the sediment, and  $\phi$  is the volumetric concentration of the mud flocs ( $\phi = c/c_{gel}$ ). At  $\phi=1$ , the sedimentation process changes from hindered settling into consolidation. The parameter  $m$  is an empirical parameter, which accounts for non-linear effects. When non-linearity is taken into account, all effects generated by a particle settling in a suspension are incorporated. Dankers (2006) concluded that an  $m$  value of 2 in Eq. (6) to be a good estimate. Equation 6 is valid in the hindered settling regime of mono-dispersed particles, and can therefore be applied when sand and silt particles

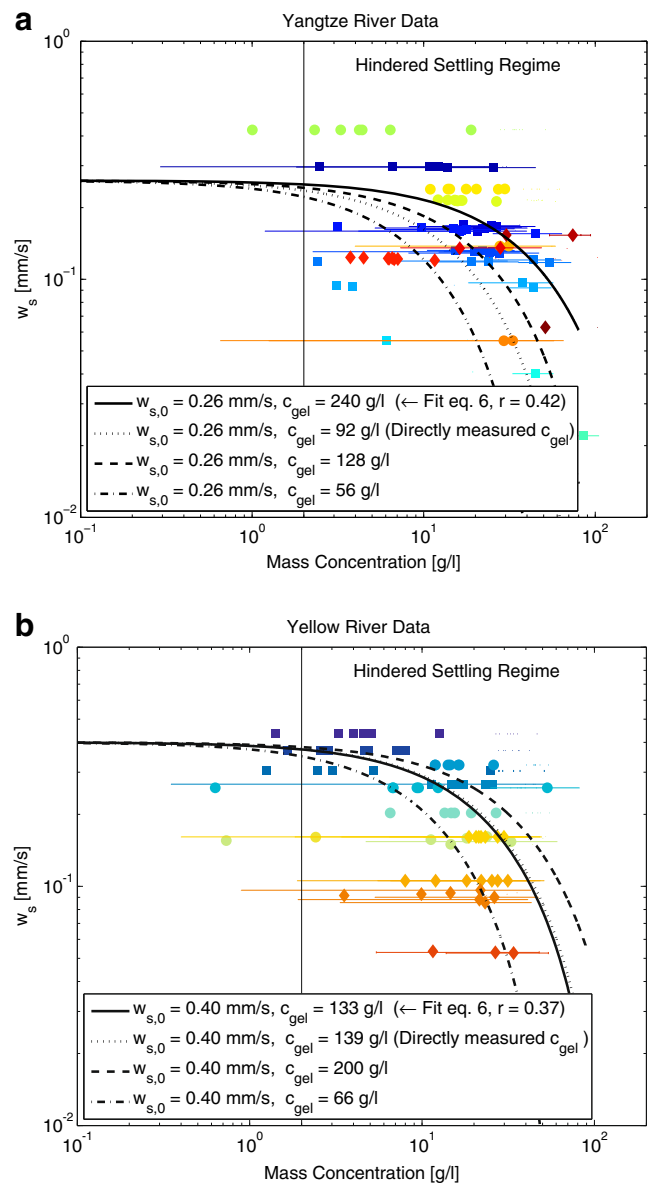


**Fig. 11** Observed still water settling velocities of flocculated material as function of the measured sediment concentration in Yangtze Estuary columns (a) and Yellow River Columns (b). Varying colors represent different test series, whereas shape variations represent different columns

have already settled (i.e. after  $t_2$ ). This always holds for the upper interface. Fitting of  $w_{s,0}$  and  $c_{gel}$  in Eq. 6 with the measured  $w_s$  and  $\phi$ , using  $m=2$ , result in gelling concentrations of 240 and 133 g/l for the Yangtze Estuary and Yellow River clay–water mixture with corresponding values for  $w_{s,0}$  of 0.26 and 0.40 mm/s, respectively; these values are much larger than obtained above.

### 5.3.2 Hindered settling of granular material

Settling velocities as function of the measured mass concentration are determined by the slope of the isolutes for

Yangtze Estuary sediment and Yellow River sediment (Fig. 12). The connected points represent the measured settling velocities within a single experiment. First, both figures show increasing effective settling velocities with concentration; the slope of the  $w_s-c$  line is positive. With further increasing concentration settling velocities reduce; the slope of the  $w_s-c$  line approaches 0 or even becomes negative. This decrease in settling velocity with increasing concentration indicates hindered settling effects. Both for Yangtze Estuary and Yellow River sediment, the transition from increasing to decreasing settling velocities occur at

mass concentration of approximately 150 - 200 g/l. It can be seen that effective settling velocities in column H are larger which is attributed to the relatively large size of the individual particles (Fig. 7).

The regime in which particles settle can be derived from the slope in the  $w_s-c$  plots (Fig. 12). A positive slope indicates descending diverging isolutes in the  $h-t$  plane of the corresponding experiment (the example in Fig. 6 shows diverging isolutes). In this regime the settling velocity is a function of the particle size (Zanke 1997). The lower initial concentrations show the largest settling velocities, as well as the largest range in settling velocities. The highest fall velocities are measured earlier in the sedimentation experiment (Fig. 6). We attribute this observation to segregation; the largest particles settle faster with higher velocities. From these observation we conclude that a positive slope in the  $h-t$  plane represent normal settling (unhindered).

A transition from positive to negative slopes in the  $w_s-c$  plane is observed around concentration of 150–200 g/l in columns A, B, J and K. In columns C and H, no clear transitions are found. Zero (constant  $w_s$ ) or negative slopes indicate parallel descending isolutes or descending converging isolutes in the  $h-t$  plane, respectively. For granular material, the Richardson and Zaki (1954) expression for reduced fall velocity is presented by:

$$w_s = w_{s,0}(1 - c/c_{bed})^n \tag{7}$$

Where for  $c_{bed}$  the volume concentration of immobile sediment is used (1,600 kg/m<sup>3</sup> based on the volume concentrations of the deposited beds in Fig. 7). The decrease in  $w_s$  with  $c$  (using three arbitrary values of  $w_{s,0}$  within the here measured range and  $n=4$ ; see Fig. 12) correspond with observations above  $c \approx 150-200$  g/l, indicating hindered settling. From the  $d_{50}$  profiles in Fig. 7 we observed segregation in all granular layers confirming that within the hindered settling regime, differential settling occurs based on particle size. Particle sizes corresponding to the hindered settling measurements in Fig. 12 are found to be in the order of 30–70  $\mu\text{m}$ .

### 5.4 Consolidation

Conductivity measurements in columns M and O failed (explained in Section 3.3). However, particle size analysis shows that vertical segregation did not occur in these columns (Fig. 7). As a result of the relatively high clay contents, a network structure of flocs is formed capturing interstitial material. In such fully cohesive conditions, material functions can be derived by applying existing consolidation theories following Merckelbach (2000), as will be elaborated below.

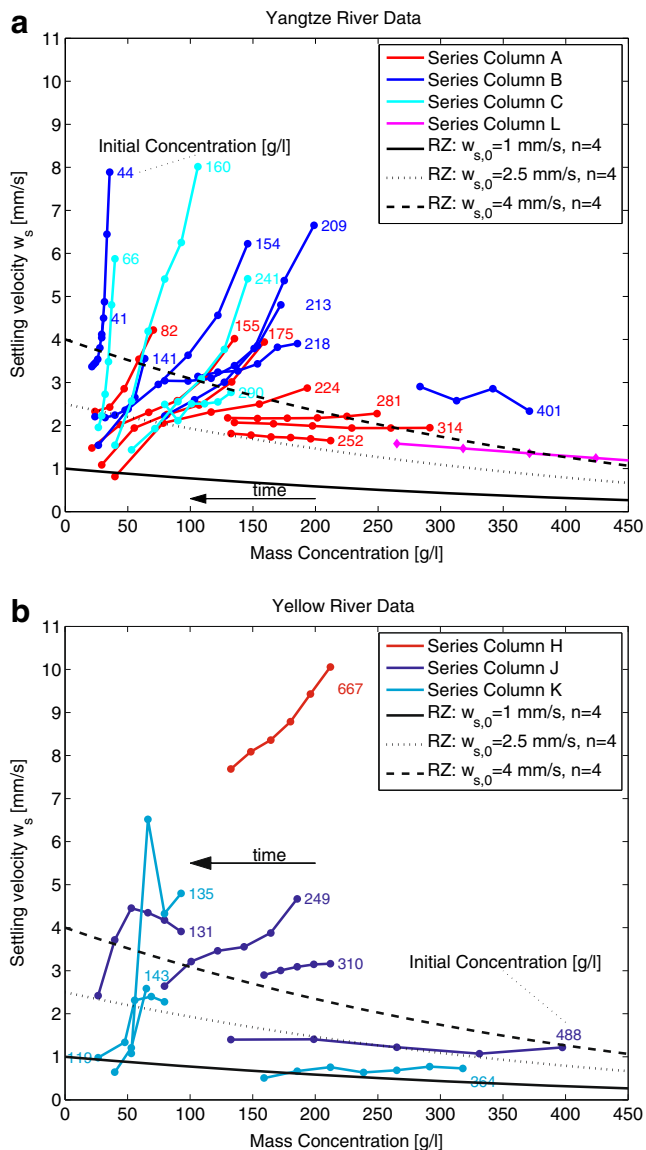


**Fig. 12** Measured settling velocities of granular material as function of the measured concentration in Yangtze River columns (a) and Yellow River Columns (b). Numbers indicate the initial concentration (in gramme per litre). All settling velocities from column H increase with concentration and are mainly found above 10 mm/s which. In order to improve the resolution of (b), settling velocities above 10 mm/s are not presented

Due to their cohesive character, clay particles in suspension tend to form aggregates. Krone (1962) noted that clay particles (primary particles) form flocs, which can join to form floc aggregates. These floc aggregates (or flocculi) can join to form larger aggregates, and so on (Merckelbach et al. 2002). This process can be mathematically described using fractal dimensions. Assuming a bed built from fractal structures (deposited mud flocs); it is assumed that the bed structure itself also exhibits fractal properties. Figure 7 shows little vertical segregation in columns M and O and a homogeneous clay fraction exceeding 10 %. Therefore, the mixture deposits as a composite mixture of which the sediment behaviour is considered to be homogeneous. Merckelbach (2000) studied the behaviour of consolidating mud layers. From different stages of (hindered) settling and consolidation physically founded equations for permeability and effective stress are derived (material functions), which solve the Gibson equation (Gibson et al. 1967). These equations are applicable when the behaviour of soft sediment is dominated by clay, but the sediment may also contain small fractions of silt and sand.

From plots of the sediment–water interface versus time on double logarithmic scales (Fig. 13), the permeability parameter ( $K_k$ ) and the fractal dimension ( $n_f$ ) can be determined (Merckelbach 2000). In both columns, the largest initial density was above the structural density, and hence in a consolidating stage from  $t_0$ . For these curves, consolidation characteristics for the initial stage of consolidation (small effective stresses) can be determined by fitting Eq. (8):

$$h(t) = \left( \frac{2-n}{1-n} \zeta_m \right)^{\frac{1-n}{2-n}} \left( (n-2)K_k \frac{\rho_s - \rho_w}{\rho_w} \right)^{\frac{1}{2-n}} t^{\frac{1}{2-n}} \quad (8)$$

For all other experiment material functions can be determined from the settling phase by fitting Eq. (9):

$$h(t) = \frac{\zeta_m}{\phi_{s,0}} - \phi_{s,0}^{1-n} K_k \frac{\rho_s - \rho_w}{\rho_w} t \quad (9)$$

Where  $\zeta_m$  is the Gibson height,  $\phi_{s,0}$  is the solid volume fraction at  $t_0$ ,  $h$  is the height of the sediment–water interface, and  $n=2/(3-n_f)$ . Effective settling velocities of the mixture are determined by taking the first derivative from the initial settling curves in Fig. 13. Gelling concentrations can be determined on the basis of the mass balance of the settling mixture and from average concentration above and below the lower interface (Dankers 2006). All experimentally derived parameters are shown in Table 5.

The consolidation characteristics obtained from fully cohesive behaving sediment in columns M and O allow a comparison with cohesive sediment from other sources. Earlier consolidation experiments are described and analysed by, e.g. Merckelbach et al. (2002) and Been (1980). These authors

studied the consolidation behaviour of mud layers without sand. Merckelbach found  $K_k$  values of in the range  $10^{-14}$  to  $10^{-16}$  m/s with fractal dimensions between 2.72 and 2.75. Perfectly spherical flocs with no interstitial pore space would have  $n_f=3$ . When in suspension, the fractal dimension of mud flocs is generally around  $n_f \approx 2$ . Therefore, the fractal dimension in a consolidating is generally more close to 3. Results of present fractal dimension computations (Table 5) show an increase in fractal dimension with increasing initial concentration, which was found by Merckelbach as well. Values found for  $n_f$  are in the same order of magnitude as was found by Merckelbach whereas the values for  $K_k$  are one order of magnitude larger ( $10^{-13}$  to  $10^{-15}$  m/s). This implies that for Yangtze Estuary fresh clay deposits consolidate faster than the Ems-Dollar sediment tested by Merckelbach.

### 5.5 Pore water pressure dissipation

In order to meet the one-dimensional volume balance equation of a settling sediment–water mixture, pore fluid has to move in opposite direction as the sediment. When the permeability of a soil is sufficiently large, the excess pore water pressure gradients are dissipated within the timescale of the settling process. In columns A, C, H and J we measured these pore water pressures. We observed that in the granular layer, excess pore water pressure gradients ( $dp_e/dz=0$ ) are negligible in contrast to the with depth linear increasing gradients in the overlying clay-dominated mixture. A lower limit for the permeability of the granular layer can be estimated from the excess pore water pressure dissipation in the initial stage after deposition following Darcy's law:

$$p_w = \rho g z \quad (10)$$

Where  $z$  is the depth in the column and  $p_w$  is the hydrostatic pore water pressure, which can be substituted by the excess pore water pressure gradient  $p_e$  when differentiated to time. The volume balance required that the settling velocity of the granular material equals the fluid velocity leading to:

$$\frac{dp_w}{dt} = \rho g \frac{dz}{dt} \Leftrightarrow \frac{dp_e}{dt} = -\rho g u \quad (11)$$

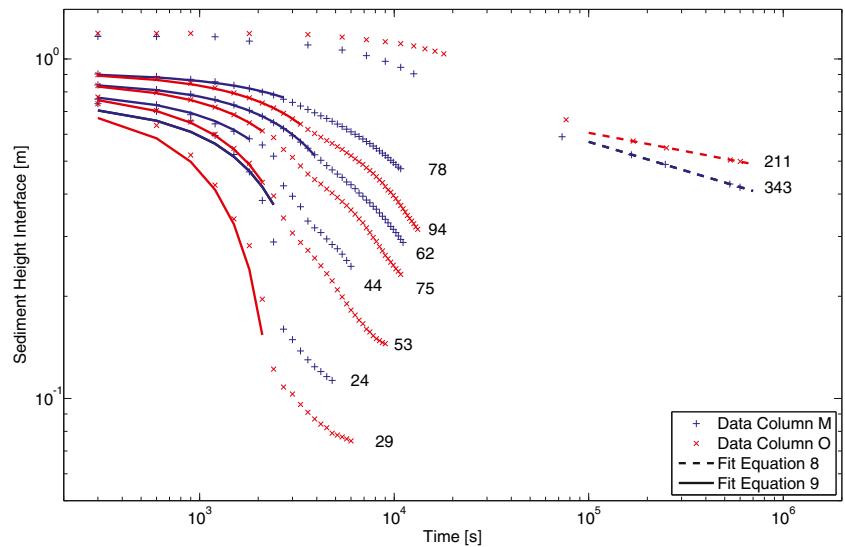
Next, by integrating over the depth of the granular layer, the fluid velocity can be determined:

$$u = - \int_0^{z_{\text{gran}}} \left( \frac{dp_e}{dt} + \frac{1}{\rho g} \right) dz \quad (12)$$

Pore water velocities are normalized with the thickness of the corresponding granular layers (Fig. 14). The largest fluid velocities are measured during the first 2 to 3 h of the sedimentation experiments.



**Fig. 13** Settling and consolidation curves for columns M and O. Numbers indicate the initial concentration (in gramme per litre)



The permeability of a soil is a measure for the rate at which pore water pressure gradients can be dissipated. The permeability of sand (order  $10^{-5}$ – $10^{-4}$  m/s) is generally much larger than that of clayey soils (order  $10^{-12}$ – $10^{-10}$  m/s) whereas the permeability of silts are found in-between (Lambe and Whitman 1979). The computed fluid velocities (Fig. 14) are an indication for the upper limit of the permeability of the granular layer. The largest fluid velocities are observed at the beginning of the test between times  $t_0$  and  $t_2$ . These velocities are generated by the dissipation of excess pore water pressure in the last stage of sedimentation of the granular material. The dissipation of excess pore water pressure in the granular layer is arrested by the overlying consolidating clay–water mixture. From the material functions (permeability parameter  $K_k$  and the fractal dimension in the bed  $n_f$ ) obtained by the fits on the settling and consolidation curves (Fig. 13) the permeability

of Yangtze Estuary clay can be determined as function of the solids contents (Merckelbach 2000):

$$k_{\text{clay}} = K_k \left( \frac{\phi_s^m}{1 - \phi_s^{\text{sa}}} \right)^{-\frac{2}{3-n_f}} \tag{13}$$

Where  $\phi_s^m$  is the combined solid content of silt and clay particles and  $\phi_s^{\text{sa}}$  is a correction for the solid content of the sand fraction. In addition, the permeability of the deposited silt layer is determined by making use of a slightly modified Kozeny–Carman Equation (10) (Carrier 2003). Here  $C_{kc}$  is a constant,  $\mu$  is the viscosity of the pore water and  $S$  is the specific surface area of the sediment. In order to compute the specific surface area of the granular layer in columns A, C, H and J, the average grain size distribution of the granular layer is applied.

$$k_{\text{silt}} = C_{kc} \frac{g}{\mu \rho} \frac{1}{(\rho_s - \rho_w)^2} \frac{1}{S^2} \left( \frac{1 - \phi_s^3}{\phi_s^2} \right) \tag{14}$$

The largest permeability of the granular beds is computed for the sediment with the largest  $d_{50}$  (Table 3). The permeability of the granular material varies only one order of magnitude between loose and dense packing, whereas clayey soils can vary up to 6–7 orders of magnitude within the same  $\phi_s$  range. The permeability of the Yangtze Estuary clay mixture is smaller than the permeability of the Yangtze Estuary silt (Fig. 15).

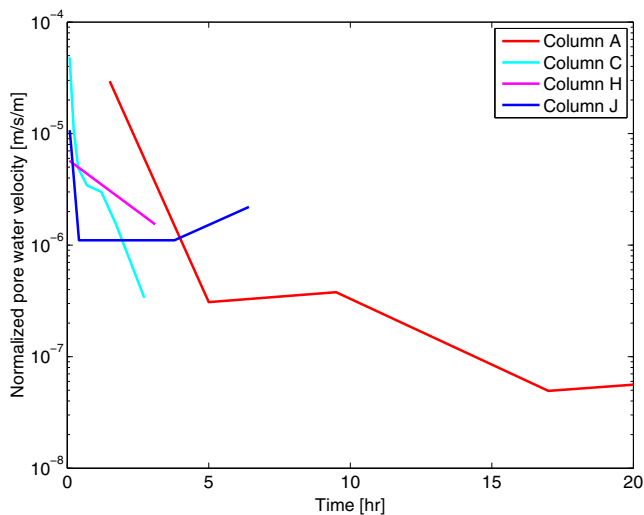


**Fig. 14** Pore water velocities normalized with the thickness of the deposited layer in columns A, C, H and J

## 6 Discussion

### 6.1 Dynamics of solids

#### 6.1.1 Consolidation

Density development in sediment deposits is a result of consolidation and/or compaction. Consolidation is the

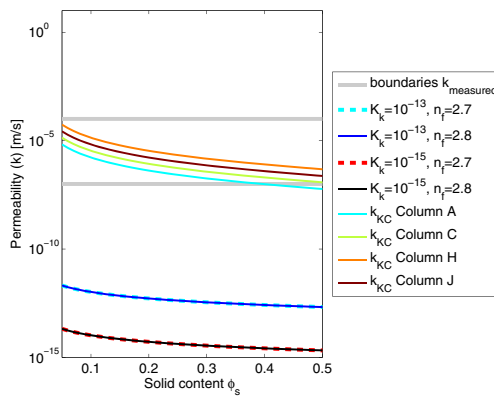


**Fig. 15** Permeability of Yangtze Estuary clay (following Eq. 11 using material functions found from fit in Fig. 13) and modelled Kozeny–Carman permeability of deposited silt in columns A, C, H and J (following Eq. 12) as function of the solid fraction. Grey solid lines indicate the boundaries of measured pore water velocities from Fig. 14

process after deposition where pore water is driven out of flocs and the space in between flocs. Strictly following this definition, silt deposits cannot consolidate since silt does not flocculate, and silt particles do not contain water. However, the permeability of fine silt is low [ $10^3$ – $10^4$  orders of magnitude lower than sand (Lambe and Whitman 1979)], and therefore pore water is expelled more slowly from fine silt deposits. Additionally, restructuring of the packing of granular material may also lead to a density increase in time. We refer to these processes as pseudo-consolidation to differentiate from the physical consolidation process in fully cohesive sediment which is governed by outflow of pore water only. Differentiating these mechanisms is difficult in non-homogeneous sediment mixtures. Nonetheless, our results show varying consolidation behaviour which can be attributed to varying sediment compositions.

The structural density or gelling concentration depends on the type of network structure that is formed. According to Van Ledden et al. (2004) a water–sediment mixture is dominated by the clay–water matrix when the clay content exceeds 5–10 %. We measured a large range of densities for  $\rho_{\text{struct}}$  and  $c_{\text{gel}}$  (Fig. 9) in sediment which is indicated as silt-dominated, based on the sediment fraction distribution. An important observation is that for  $\psi_{\text{si}} > 70$  %, the porosity (both in the field and in the settling columns) mostly exceeds 60 %. Such high porosities indicate that the network structure is dominated by a clay–water matrix, whereas sediment fraction analyses would suggest a silt-dominated skeleton. The high porosities we found are related to relatively short consolidation periods. Even though the clay content may be low ( $7 \% < \psi_{\text{cl}} < 25$  %), the permeability of silt is so low that the porosity of the silt–water mixture only slowly decreases. Potentially, the amount of silt is large enough to form a silt-dominated network structure. In order to reach a state where the silt particles form the skeleton,

more water has to be expelled from the pores of the clay minerals.

In our settling columns, we measured density development in layers with varying sediment composition in columns A, B, C, H, J and K. Therefore, we distinguish between layers based on the dominant sediment fraction. We refer to sand dominated when  $\psi_{\text{sa}} > 67$  % (shaded area A in Fig. 1) and to clay dominated when  $\psi_{\text{cl}} > 10$  % (areas II, IV and V in Fig. 1). Both conditions are in analogy with Van Ledden et al. (2004). For silt-dominated sediment we apply two conditions:  $\psi_{\text{cl}} < 10$  % and  $\psi_{\text{si}} > 50$ –60 %, indicated by area VI in Fig. 1. Results of density development within these layers are shown in Table 6.

The density of sand-dominated sediment remains fairly constant, whereas the density of the clay-dominated sediment continuously increases. The silt-dominated sediment shows small density increments, which already occur during the first 2–3 h of the experiment, which corresponds with the timeframe in which the largest excess pore water pressures dissipate. In columns H and J only small solid fraction increments ( $\Delta\phi_s \approx 0.005$ – $0.01$ ) are observed over the first 5 days. The in situ porosities are generally smaller, which is attributed to a longer consolidation period. For quartz particles with mean diameter ( $d_m$ ) of 5.7  $\mu\text{m}$ , Roberts et al. (1998) found a density increase from 1,710 to 1,775  $\text{kg/m}^3$  ( $\approx 4$  % of a solid fraction increase from 0.43 to 0.47) in 2.5 days, after which density development rates reduced significantly.

We conclude that pseudo-consolidation occurs in natural silt-dominated sediment in the form of pore water dissipation within the first 2–3 h after deposition. After that, consolidation rapidly slows down. The porosity variation in silt-dominated sediment between in situ and laboratory measurements deviate approximately 5 %. This indicates that after the first 2–3 h consolidation only slowly continues. During this secondary consolidation phase, either pore water is being expelled from the interstitial clay flocs, or compaction is significantly delayed by the low permeability of the silt fraction. The small density increase indicates that little

**Table 6** Solid fraction increase in sand-, silt- and clay-dominated layers with the corresponding timeframe

Column	Sand dominated $\psi_{\text{sa}} > 70$ %		Silt dominated $\psi_{\text{cl}} < 10$ %, $\psi_{\text{si}} > 50$ %		Clay dominated $\psi_{\text{cl}} > 10$ %	
	$\Delta\phi_s$	$\Delta t$ (h)	$\Delta\phi_s$	$\Delta t$ (h)	$\Delta\phi_s$	$\Delta t$ (h)
A	–	–	0.005	24	0.01	24
B	–	–	0.005	0.5	0.01	7
C	0	3.5	0.005	2.5	0.03	3.5
H	0	124	0.005	124	–	–
J	0.002	166	0.01	166	0.06	166
K	0	47	0.01	1	0.02	47

clay is present in the bed to influence consolidation and sedimentation processes.

The behaviour of the overlying clay–water mixture follows generally accepted theories on settling and consolidation for cohesive sediment. A comparison between the overlying consolidation clay–water mixture and the underlying granular layer between  $t_3$  and  $t_{end}$  show the largest transition in consolidation behaviour around clay percentages of 8–10 % in columns A, B, C, H and J. Maximum clay fractions at which consolidation behaviour does not alter into cohesive consolidation can be found between 5–10 %. In column M and O, where consolidating is according to generally accepted cohesive sediment consolidation theories, clay percentages of approximately 12 % are found. Therefore, we conclude that the transition between cohesive and non-cohesive consolidation can be related to clay percentages of around 10 % in the Yangtze estuary and Yellow River sediments.

This implies that in dynamic environments (when sediment is regularly resuspended), and where the sediment mixture is silt-dominated (based on sediment fraction analysis) and clay contents exceed 10 %, the network structure is dominated by the clay–water matrix. A sharp increase in porosity is observed both in the field and in settling columns when the clay content exceeds 10–12 %. Again, in situ porosities are smaller ( $\approx 15\%$ ) than settling column porosities. For  $\psi_{cl} < 10\%$ , in situ porosities deviate only little ( $\approx 5\%$ ) from the theoretical porosity for those sediment fraction composition as defined in the silt-dominated area of Fig. 1. Therefore, sediment below this threshold can already be classified as a soil, whereas the sediment above this threshold is still dominated by the clay–water matrix, thereby defining the transition from cohesive to non-cohesive behaviour. Therefore, we conclude that area V in Fig. 1 may only be referred to as silt-dominated when fully consolidated. In the non-cohesive silt-dominated area (VI) the measured porosities (both in situ and laboratory) match the theoretical porosities based on sediment fraction Van Ledden et al. (2004) of silt-dominated sediment well for  $\psi_{cl} < 10\%$ , although the porosity of recently deposited sediments are somewhat smaller, which is attributed to a small consolidation potential.

### 6.1.2 Gelling concentration

Four methods were used to compute the gelling concentration/structural density (Table 7). Dankers (2006) concluded that direct measurement of  $c_{gel}$  is the most reliable and that the mass balance method overestimates  $c_{gel}$ . Based on the results in Table 7 we conclude that the Van Rijn formulation (Eq. 5) overestimated  $c_{gel}$  as well. The fit of Eq. 6 on the measured  $w_s-c$  data shows good agreement with the measured gelling concentration of Yellow River clay. This fit on the Yangtze River data is in less good agreement with the direct measurements, probably caused by a variation in

**Table 7** Gelling concentrations of Yangtze and Yellow River clay determined with various methods

Method	Yangtze Estuary clay	Yellow River clay
Direct measurement	107±22	81±17
Mass balance	136±22	–
Fit Eq. 6 (Dankers 2006)	240, $r=0.42$	133, $r=0.37$
Computed with Eq. 5 (Van Rijn 2007)	178±51	184±25

salinity in the Yangtze River columns (A, B and C). A variation in salinity influences  $w_{s,0}$  in the settling stage of the experiment through flocculation processes: flocs sizes have a positive relation with salinity and the settling velocity of a single floc increases with floc size.

Although the gelling concentration in the Yellow River is lower than in the Yangtze River, using the direct measurement, the gelling concentration in both rivers is fairly similar. Apparent differences in measurement methodology are close to physical differences between the Yangtze and the Yellow River. Despite the different trajectories of the Yellow and Yangtze River, the mineralogy of the clay minerals show a remarkable resemblance [Table 8, based on Li et al. (1984), Ren and Shi (1986), Shiming et al. (2008), Xu et al. (2009), Yang et al. (2004)]. Even more surprising, is that the Yellow River samples were taken in a fresh water environment, whereas the Yangtze River sediment was sampled in saline/brackish water. This is in line with Guo and He (2011) who concluded from observations in the Yangtze River that freshwater flocs are not necessarily smaller than those found in saline environments. Above all, the largest factor influencing the gelling concentration appears to be the initial sediment concentration (Table 4). This is anticipated since higher initial concentrations result in larger flocs on which the gelling concentration depends. Dankers (2006) uses a mean gelling concentration in order to overcome this problem in modelling purposes.

### 6.1.3 Settling velocity

Two different settling regimes can be distinguished for the granular material. At low concentrations ( $c < 150\text{--}200$  g/l)

**Table 8** Mineral composition of Yangtze and Yellow River clay

Mineral	Yangtze River, %	Yellow River, %
Illite	66	64
Smectite	8	15
Kaolinite	12	9
Chlorite	14	12

the settling velocities increase with particle size and sediment concentration, and the sediment segregates. For  $c > 150\text{--}200$  g/l, particles settle in a hindered settling regime, where  $w_s$  decreases with increasing  $c$  and segregation is smaller. The magnitude of the measured settling velocities indicates that the material is not flocculated, which is supported by the magnitude of the gelling concentration; for concentrations exceeding  $c_{\text{gel}}$  settling velocities are still larger than 1 mm/s indicating the material is not consolidating. The settling velocities can be modelled with a modified Richardson–Zaki equation (Eq. 7) for hindered settling with  $n=4$  being characteristic for granular material (Fig. 12).

#### 6.1.4 Clay–silt ratios

Merckelbach (2000) found in his consolidation experiments that the sand fraction partially segregated from the clay and silt fraction, but the clay–silt ratio remained more or less constant at all levels above the base. He concluded that this indicated that the silt particles are not part of the flocs network structure, but merely act as space filling material. In our experiments, the clay fraction is always increasing in upward direction; since the clay fraction in the lower regions of the columns is smaller than measured in the bulk sample, clay is transported upwards by the return flow of depositing coarser particles. This vertical transportation mechanism reveals that in silt-rich environments clay and silt are not always transported simultaneously, as indicated by Van Ledden et al. (2004). In all columns, the clay content never exceeds 9 % in the granular layer. In the silt-dominated granular layer, the silt–clay ratio is approximately 9:1 whereas in clay-dominated layers the silt–clay ratio is approximately 7:1. In the overlying clay-dominated mixture the silt–clay ratio is approximately 4:1–5:1. Therefore, we conclude that in these silt-rich environments silt is not only transported while captured within flocculated clay aggregates, but also as individual particles.

#### 6.2 Dynamics of pore water

The largest dissipation rates of excess pore water pressure in the granular sub-layer are measured during the first 2–3 h of the sedimentation process. Figure 15 shows that the computed permeabilities of the granular layer correspond with the range of the measured pore water velocities. After these first hours, the fluid velocity decreases but excess pore water pressures are still present in the granular layer. Total dissipation of these excess pressures is prevented by the overlying consolidating clay–mixture. The gelling concentration of Yangtze and Yellow River clay amount to about  $\phi_s \approx 0.04\text{--}0.05$ , which indicates that around this point, the permeability of the overlying clay–water mixture is less than the permeability of the granular layer. This observation is supported

by the excess pore water profiles; these increase linearly with depth in the clay–water mixture, whereas they are constant in the granular layer, indicating an absence of pore water pressure gradients. At the granular interface, the excess pore water profiles connect and the excess pressure in the granular layer equals the maximum pressure in the bottom of the clay–water mixture. The dissipation rate of excess pore water pressure is the largest in column H, which also shows one of the largest segregation rates. Segregation of sediment prevents mixing of fine and coarser particles, and therefore pores and permeability are larger. For non-segregating material, the spaces between the particles are filled up to a larger extent with fine grains, reducing the permeability. This is reflected in the Kozeny–Carman equation by  $S$  (the specific surface area) in the denominator. Figure 15 shows that the permeability's for columns A (not segregated) and H (segregated) varies an order of magnitude.

#### 6.3 Implications

##### 6.3.1 Yellow river

Unique morphodynamic processes such as hyper-concentrated floods (HCF), mass erosion and mass deposition occur in the Yellow River as a result of the large amount of fine grained sediment with large silt contents. The median grain size of sediment from the loess plateau varies between 15 and 50  $\mu\text{m}$ , with 10–20 % clay particles (Wan and Wang 1994). Most of the samples in our experiments have a similar  $d_{50}$  and clay content. HCF's can lead to a collapse of the turbulent structure of the flow leading to high vertical sediment concentration gradients. Due to this stratification, near-bed sediment concentrations increase while near-bed flow velocities decrease, resulting in rapid sediment deposition (Van Maren et al. 2009b). During this stage, the bed may rise for several meters (Wan and Wang 1994), which is referred to as mass deposition. Our experiments showed that during deposition at concentrations approximating HCF concentrations, water remains captured in the silty bed. After deposition, this pore water is expelled from the bed within a timeframe of 2–3 h. Therefore, we conclude that within the timescale of one flood, all excess pore water is expelled from the silty sediment beds. In our experiment, the overlying clay-dominated mixture arrests the dissipation of pore water from the granular layer due to a difference in permeability. Due to the dynamic environment in riverine systems, such a layer will not be present and therefore it is anticipated that excess pore water dissipation rates will increase slightly. Within the timeframe of our experiments, no significant consolidation was measured in silt-rich sediment beds. However, a comparison between in situ porosities and laboratory porosities on sediment from the same

source shows that some consolidation ( $\approx 5\%$ ) is still possible. The small consolidation rates are ascribed to the low permeability of the silty soil.

Typical concentrations at the onset of HCF are found to be 200–300 g/l. From our experiments we observed that hindered settling of the silt fraction already occurs at concentration around 150–200 g/l. Interestingly, a concentration of  $\sim 150$  g/l is also the critical concentration in the stability diagram developed for HCF in the Yellow River (Van Maren et al. 2009a). At concentrations exceeding 150 g/l, the flow velocity required to hold sediment in suspension decreases resulting in vertically uniform sediment concentration profiles and rapid erosion rates. Below these concentrations, both silty and granular material settle under normal conditions, e.g. larger particles settle faster than the smaller ones resulting in strong segregation. Within the hindered settling regime, segregation of granular material is limited, and can even be absent, resulting in a more evenly distributed PSD in the deposited bed. This implies, following the Kozeny–Carman permeability relating to the specific surface area, that the permeability of the bed is homogenous.

### 6.3.2 Yangtze River

The high number of dams constructed in the Yangtze River catchment area influence sediment properties in the downstream direction, both in discharge and size. Van Maren et al. (2013) hypothesize that these reservoirs most strongly influence the silt fraction because sand and silt is mostly trapped within the reservoirs (and the clay fraction is flushed through), while sand is resuspended from the downstream river bed. A possible effect they anticipate is that the Yangtze River mouth may become depleted of silt. The results obtained from present study gain insight to the impact of such a removal of silt on the silt-dominated Yangtze Estuary tidal flats.

Removal of silt from a clay–silt–sand mixture will lead to relatively higher clay fractions, and therefore the clay content will more easily exceed the critical 10 % (above which we observed fully cohesive consolidation behaviour) on Chongming’s northern tidal flats. This may have several contrasting impacts on erosion behaviour. First, the erosion rate of cohesive sediment beds is typically larger than a non-cohesive sediment bed (Mitchener and Torfs 1996; Panagiotopoulos et al. 1997). At the same time, consolidation of the sand–mud mixture will take longer, resulting in larger erosion rates of poorly consolidated material. When sediment has time to consolidate, a decrease in silt content may increase the resistance to erosion, whereas the resistance to erosion may decrease when sediment has little time to consolidate. Obviously the exact impact depends on the (spatially varying) mud content, with the largest resistance of erosion occurring in

sand–mud mixtures with 30–50 % mud (by weight) according to Mitchener and Torfs (1996).

A removal of the silt fraction in the sand–silt-dominated tidal flats southeast on Chongming Island will make the sediment sandier, resulting in a higher  $d_{50}$  and structural density. This implies that the sedimentation and consolidation behaviour remains non-cohesive. However, for the grain size range on these flats ( $d_{50}=30$  to  $50\ \mu\text{m}$ ), Roberts et al. (1998) demonstrated that the erosion threshold decreases with increasing grain size. In this range of particle size, the influence of bulk density on the erosion rate is larger than the influence of particle size on the erosion rate. Therefore, we expect that erosion rates on the south-eastern mudflat of Chongming Island will decrease.

### 6.3.3 Modelling of sedimentation processes

The work presented here has several implications for numerical modelling of sediment mixtures in general, but of silt-dominated mixtures in particular. This concerns the settling stage as well as the erosion stage. Multiple fractions settle at different speeds in the free settling zone, as elaborated for instance by Dankers (2006) and Manning et al. (2010). This requires multiple settling velocities, with settling of the finest fraction(s) preferentially done using a flocculation model [as advocated by Manning et al. (2010)] The cohesive behaviour of Yellow River as well as Yangtze Estuary sediments observed during our experiments suggest that flocculation is also important in silt-dominated suspensions [including fluvial environments, thereby supporting recent observations by Guo and He (2011) in the Yangtze River].

Our experiments have further shown that segregation occurs at concentrations up to 200 g/l in silt-rich sediment systems. Above this concentration, the various fractions settle in a more uniform manner, which should be correctly numerically implemented in numerical models describing these conditions. The work presented here provides observations to improve numerical modelling of hindered settling of sediment mixtures. But although an adequate description of settling velocities is important for the settling phase, it may be even more important for the subsequent erosion. Multi-fraction multi-layer models become increasingly more common (Geleynse et al. 2011; Le Hir et al. 2011; Sanford 2008). In such models, erosion of sediment layers may be strongly influenced by armouring effects resulting from deposition of poorly erodible material, and hence, correct simulation of individual settling (allowing formation of armouring layers) or mass settling is essential (especially if sand–mud interactions are accounted for).

Concentrations around 200 g/l are generally very high for natural conditions. Such conditions are typical for fluid mud and for the hyperconcentrated floods briefly described earlier. Fluid mud often forms in ports or low-energy areas

where erosion of fluid mud deposits is generally not an issue. However, erosion of sediment deposited during hyperconcentrated floods is essential for the morphodynamics of some silt-dominated rivers [with the Yellow River as the best example, see e.g. van Maren et al. (2009a; 2009b)]. The experiments described in this paper are essential to improving our quantitative description of erosion–sedimentation mechanisms in such silt-dominated systems.

## 7 Conclusions

Sedimentation experiments with silt-rich sediment from the Yellow River and Yangtze Estuary have been carried out in specially designed settling columns. These columns contain a series of vertically equidistantly placed conductivity probes and pore water outlets, in order to continuously measure vertical density profiles and time series of excess pore water pressures. This setup allows studying the physical processes of sedimentation in silt-rich sediment. Present setup allows determining material properties in two ways; structural densities, gelling concentrations and permeabilities are measured directly. Settling velocities, gelling concentrations, consolidation rates, fractal dimensions and permeability parameters are measured by applying known sedimentation theory from literature to the direct measured properties. Owing to the high flexibility and accuracy, we conclude that this setup is suitable for studying sedimentation mechanisms.

Our laboratory experiments on silt-rich sediment, in combination with fieldwork in silt-rich environments, show some general trends with respect to the effect of silt on sedimentation processes. The most important findings of the present study can be summarized in the following conclusions:

- We conclude that silt-rich sediment settles in an analogous manner as sandy material for concentration below 150 g/l; differential settling velocities lead to segregation. Between 150–200 g/l the settling regime alters into hindered settling. Now, segregation rates reduce or even vanish. Grain sizes of this material are in the range between 30 and 70  $\mu\text{m}$ .
- Segregation in silt-rich sediment systems is strongly dependent on the clay percentage and the initial concentration. In order to form a space filling clay–water mixture, the initial concentration of the clay fraction has to be close to the gelling point. For clay percentages above 10 % and small sand percentages (<5 %) the clay–water mixture is strong enough to capture interstitial material. Only 1–2 % smaller clay percentages lead to segregation of silt and sand from the clay–water matrix. For  $\psi_{cl} > 10\%$  the material shows fully cohesive consolidation

behaviour. For  $\psi_{cl} < 10\%$  and  $\psi_{si} > 50\%$  sediment shows weak cohesive behaviour due to the low permeability of the silt fraction. For  $\psi_{sa} > 70\%$  no consolidation occurs. Therefore, we conclude that the transition between cohesive and non-cohesive consolidation behaviour in silt-rich sediment occurs at a threshold in the clay content of about 10 %, which is in analogy with the threshold for cohesive and non-cohesive erosion behaviour.

**Acknowledgements** This work has been carried as part of the Sino–Dutch collaboration project ‘Effects of human activities on the ecomorphological evolution of rivers and estuaries’ funded by the Dutch Royal Academy of Sciences (KNAW) and is supported by the Natural Science Foundation of China (41130856) within the framework of Scientific Alliances between China and the Netherlands. Shi Benwei, Jin Can, Yuan Dailiang, Jiang Fengpei, Liu Jianhua, Zhao Jie, Zhu Lei, Pieter Leo, Yuan Lin, Richard de Reus, Christian Schwarz, Tian Xin, Ming Yang and Tom Ysebaert are acknowledged for their assistance during the fieldwork and laboratory experiments.

## References

- Ariathurai CR, Arulanandan K (1978) Erosion rates of cohesive soils. *ASCE, J Hydraul Div* 104(2):279–282
- Been K (1980) Stress-strain behaviour of a cohesive soil deposited under water. DPhil, University of Oxford.
- Been K, Sills GC (1981) Self-weight consolidation of soft soils: an experimental and theoretical study. *Geotechnique* 31(4):519–535
- Blewett J, McCarter WJ, Chrisp MT, Starss G (2001) Monitoring sedimentation of a clay slurry. *Geotechnique* 51(8):723–728
- Bowden RK (1988) Compression behaviour and shear strength characteristics of a natural silty clay sedimented in the laboratory. Ph.D. thesis, Oxford University.
- Carrier WD (2003) Goodbye, Hazen; Hello, Kozeny–Carman. *J Geotech Geoenviron Eng* 129(11):1054–1056
- Chen J, Wang F, Xia X, Zhang L (2002) Major element chemistry of the Changjiang (Yangtze River). *Chem Geol* 187(3–4):231–255
- Cuthbertson A, Dong P, King S, Davies P (2008) Hindered settling velocity of cohesive/non-cohesive sediment mixtures. *Coast Eng* 55(12):1197–1208
- Cuthbertson AJS, Dong P, Davies PA (2010) Non-equilibrium flocculation characteristics of fine-grained sediments in grid-generated turbulent flow. *Coast Eng* 57(4):447–460
- Dai Q, Shan HX, Jia YG, Meng XM (2009) Laboratory study on the relationship between suspended sediment concentration and electrical conductivity, Proceedings of the ASME 2009 28th International Conference on Ocean, Offshore and Arctic Engineering College of Environmental Science and Engineering Qingdao, China
- Dankers PJT (2006) On the hindered settling of suspensions and mud-sand mixtures. Ph.D. thesis, Delft University of Technology
- Dankers PJT, Winterwerp JC (2007) Hindered settling of mud flocs: theory and validation. *Cont Shelf Res* 27(14):1893–1907
- Floss R (1970) Vergleich der Verdichtungs- und Verformungseigenschaften unstetiger und stetiger Kiessanden hinsichtlich ihrer Eignung als ungebundenes Schuttmaterial in Strassenbau. *Wissenschaftliche Berichte der Bundesanstalt für Strassenwesen*, Heft, 9

- Geleynse N, Storms JEA, Walstra DR, Jagers HRA, Wang ZB, Stive MJF (2011) Controls on river delta formation; insights from numerical modelling. *Earth Planet Sci Lett* 302(1–2):217–226
- Gibson RE, England GL, Hussey MJL (1967) The theory of one-dimensional consolidation of saturated clays. *Geotechnique* 17(3):261–273
- Guo L, He Q (2011) Freshwater flocculation of suspended sediments in the Yangtze River, China. *Ocean Dyn* 61(2):371–386
- He MC, Sun Y, Li XR, Yang ZF (2006) Distribution patterns of nitrobenzenes and polychlorinated biphenyls in water, suspended particulate matter and sediment from mid- and down-stream of the Yellow River (China). *Chemosphere* 65(3):365–374
- Jacobs W (2011) Sand-mud erosion from a soil mechanical perspective. Ph.D. thesis, Delft University of Technology
- Jin L, McNeil J, Lick W, Gailani J (2002) Effects of bentonite on the erosion rates of quartz particles. University of California: Mechanics and Environmental Engineers, Santa Barbara
- Krone RB (1962) Flume studies of the transport of sediment in estuarial shoaling processes. University of California, Berkeley
- Kuerbis R, Negussey D, Vaid YP (1988) Effect of gradation and fines content on the undrained response of sand. *Hydraulic Fill Structures (GPS21)*:330–345.
- Lambe TW, Whitman RV (1979) *Soil Mechanics*. SI Version, New York
- Le Hir P, Cayocca F, Waeles B (2011) Dynamics of sand and mud mixtures: a multiprocess-based modelling strategy. *Cont Shelf Res* 31(10, Supplement):S135–S149
- Li YH, Hisayuki T, Yang TS, Chen JS (1984) The elemental composition of suspended particles from the Yellow and Yangtze Rivers. *Geochim Cosmochim Acta* 48(7):1561–1564
- Manning AJ, Baugh JV, Spearman JR, Pidduck EL, Whitehouse RJS (2011) The settling dynamics of flocculating mud-sand mixtures: part 1: empirical algorithm development. *Ocean Dyn* 61(2–3):311–350
- Manning AJ, Baugh JV, Spearman JR, Whitehouse RJS (2010) Flocculation settling characteristics of mud: sand mixtures. *Ocean Dyn* 60(2):237–253
- Merckelbach LM (2000) Consolidation and strength evolution of soft mud layers. Ph.D. thesis, Delft University of Technology
- Merckelbach LM, Kranenburg C, Winterwerp JC (2002) Strength modelling of consolidating mud beds. *Proceedings in Marine Science*. Elsevier, Amsterdam, pp 359–373
- Mitchener H, Torfs H (1996) Erosion of mud/sand mixtures. *Coast Eng* 29:1–25
- Montserrat F, Van Colen C, Provoost P, Milla M, Ponti M, Van den Meersche K, Ysebaert T, Herman PMJ (2009) Sediment segregation by biodiffusing bivalves. *Estuarine Coastal Shelf Sci* 83(4):379–391
- Panagiotopoulos I, Voulgaris G, Collins MB (1997) The influence of clay on the threshold of movement of fine sandy beds. *Coast Eng* 32(1):19–43
- Partheniades E (1962) A study of erosion and deposition of cohesive soils in salt water. Ph.D. thesis, University of California
- Ren ME, Shi YL (1986) Sediment discharge of the Yellow River (China) and its effect on the sedimentation of the Bohai and the Yellow Sea. *Cont Shelf Res* 6(6):785–810
- Richardson JF, Zaki WN (1954) The sedimentation of a suspension of uniform spheres under conditions of viscous flow. *Chem Eng Sci* 3(2):65–73
- Roberts J, Jepsen R, Gotthard D (1998) Effects of particle size and bulk density on erosion of quartz particles. *J Hydraul Eng* 124:1261
- Sanford LP (2008) Modeling a dynamically varying mixed sediment bed with erosion, deposition, bioturbation, consolidation, and armoring. *Comput Geosci* 34(10):1263–1283
- Shields A (1936) *Anwendung der Ähnlichkeits Mechanik und der Turbulenzforschung auf die Geschiebe Bewegung*. Preuss. Versuchsanstalt für Wasserbau und Schiffbau, Berlin, 20 p
- Shiming W, Anchun L, Kehui X, Xueming Y (2008) Characteristics of clay minerals in the Northern South China Sea and its implications for evolution of East Asian Monsoon since Miocene. *J China Univ Geosci* 19(1):23–37
- Sorensen JA, Glass GE (1987) Ion and temperature dependence of electrical conductance for natural waters. *Anal Chem* 59:1594–1597
- Terzaghi K, Frohlich OK (eds) (1936) *Theorie der Setzung von Tonschichten; eine Einführung in die analytische Tonmechanik*. Franz Deuticke, Leipzig
- Torfs H, Mitchener H, Huysentruyt H, Toorman E (1996) Settling and consolidation of mud/sand mixtures. *Coast Eng* 29(1–2):27–45
- Van Ledden M, Van Kesteren WGM, Winterwerp JC (2004) A conceptual framework for the erosion behaviour of sand–mud mixtures. *Cont Shelf Res* 24(1):1–11
- Van Maren D (2007) Grain size and sediment concentration effects on channel patterns of silt-laden rivers. *Sediment Geol* 202(1–2):297–316
- Van Maren DS, Winterwerp JC, Wang ZY, Pu Q (2009a) Suspended sediment dynamics and morphodynamics in the Yellow River, China. *Sedimentology* 56(3):785–806
- Van Maren DS, Winterwerp JC, Wu BS, Zhou JJ (2009b) Modelling hyperconcentrated flow in the Yellow River. *Earth Surf Process Landforms* 34(4):596–612
- Van Maren DS, Yang SL, He Q (2013) The impact of silt trapping in large reservoirs on downstream morphology: the Yangtze River. *Ocean Dyn.* (in review)
- Van Rijn LC (1984) Sediment transport, part i: bed load transport. *J Hydraul Eng* 110(10):1431–1456
- Van Rijn LC (2007) Unified view of sediment transport by currents and waves. I: initiation of motion, bed roughness, and bed-load transport. *J Hydraul Eng* 133(6):649–667
- Wan Z, Wang Z (1994) *Hyperconcentrated Flow*. IAHR monograph, Balkema: Rotterdam: 230.
- Winterwerp J, Van Kesteren W (2004) *Introduction to the physics of cohesive sediment in the marine environment*. Elsevier, Amsterdam
- Winterwerp JC (2001) Stratification of mud suspensions by buoyancy and flocculation effect. *J Geophys Res* 106(10):22
- Wu B, Wang G, Ma J, Zhang R (2005a) Case study: river training and its effects on fluvial processes in the Lower Yellow River, China. *J Hydraul Eng* 131(2):85–96
- Wu L, Huh Y, Qin J, Du G, van Der Lee S (2005b) Chemical weathering in the Upper Huang He (Yellow River) draining the eastern Qinghai-Tibet Plateau. *Geochim Cosmochim Acta* 69(22):5279–5294
- Xia XH, Yang ZF, Huang GH, Zhang XQ, Yu H, Rong X (2004) Nitrification in natural waters with high suspended-solid content. A study for the Yellow River. *Chemosphere* 57(8):1017–1029
- Xu J (2007) Trends in suspended sediment grain size in the upper Yangtze River and its tributaries, as influenced by human activities. *Hydrol Sci J* 52(4):777–792
- Xu K, Milliman JD, Li A, Paul Liu J, Kao S-J, Wan S (2009) Yangtze- and Taiwan-derived sediments on the inner shelf of East China Sea. *Cont Shelf Res* 29(18):2240–2256
- Yang SY, Jung HS, Li CX (2004) Two unique weathering regimes in the Changjiang and Huanghe drainage basins: geochemical evidence from river sediments. *Sediment Geol* 164(1–2):19–34
- Zanke UCE (1997) *Berechnung der Sinkgeschwindigkeiten von Sedimenten*. Technical University, Hannover